

494954

13P

In Pm, 7/2K

1

Revised and Submitted to the *Journal of Geophysical Research*, June 2000.

Atmospheric sulfur cycle simulated in the global model GOCART: Model description and global properties

Mian Chin,^{1,2} Richard B. Rood,² Shian-Jiann Lin,² Jean-Francois Müller,³
and Anne M. Thompson²

Abstract

The Georgia Tech/Goddard Global Ozone Chemistry Aerosol Radiation and Transport (GOCART) model is used to simulate the atmospheric sulfur cycle. The model uses the assimilated meteorological data from the Goddard Earth Observing System Data Assimilation System (GEOS DAS). Global sulfur budgets from a 6-year simulation for SO₂, sulfate, dimethylsulfide (DMS), and methanesulfonic acid (MSA) are presented in this paper. In a normal year without major volcanic perturbations, about 20% of the sulfate precursor emission is from natural sources (biogenic and volcanic) and 80% is anthropogenic; the same sources contribute 33% and 67% respectively to the total sulfate burden. A sulfate production efficiency of 0.41-0.42 is estimated in the model, an efficiency which is defined as a ratio of the amount of sulfate produced to the total amount of SO₂ emitted and produced in the atmosphere. This value indicates that less than half of the SO₂ entering the atmosphere contributes to the sulfate production, the rest being removed by dry and wet depositions. In a simulation for 1990, we estimate a total sulfate production of 39 Tg S yr⁻¹, with 36% and 64% respectively from in-air and in-cloud oxidation of SO₂. We also demonstrate that major volcanic eruptions, such as the Mt. Pinatubo eruption in 1991, can significantly change the sulfate formation pathways, distributions, abundance, and lifetime. Comparison with other models shows that the parameterizations for wet removal or wet production of sulfate are the most critical factors in determining the burdens of SO₂ and sulfate. Therefore, a priority for future research should be to reduce the large uncertainties associated with the wet physical and chemical processes.

1. Introduction

The important roles of sulfate aerosol in climate change, atmospheric chemistry, and environmental health have been well recognized in recent years. Sulfate aerosol is one of the major aerosol types in the troposphere with a dominant anthropogenic component. It affects the Earth's radiative balance directly by scattering solar radiation and indirectly by forming new clouds and modifying cloud properties. It also provides surfaces for heterogeneous reactions to take place, thus altering the concentrations of many important atmospheric species. Sulfate can also interact with other types of aerosols, such as dust and carbonaceous aerosols, to modify their hygroscopic properties when internally mixed with them. The fundamental step toward quantifying all the direct and indirect effects of sulfate aerosol is determining its spatial and temporal distributions and the various processes that control the distributions.

There have been numerous observational data of aerosols and their precursors obtained at ground sites, in field campaigns, and from satellite measurements. However, measurements at the surface or in field campaigns are limited in spatial or temporal coverage, while satellite observations are limited in measurable quantities. Therefore, a global model is needed to integrate the space-borne, air-borne, and ground-based data in order to interpret the data in a broader context. In fact, several global models have been used to study the tropospheric sulfur cycle since 1991 [e.g., Langner and Rodhe, 1991; Pham *et al.*, 1995; Feichter *et al.*, 1996; Chin *et al.*, 1996; Chuang *et al.*, 1997; Roelofs *et al.*, 1998; Koch *et al.*, 1999; Barth *et al.*, 2000; Rasch *et al.*, 2000]. Almost all the published global sulfur models were either driven by the off-line meteorological fields generated in general circulation models (GCM), or were coupled on-line with the GCM. Although these model studies have helped to advance our understanding of tropospheric sulfur cycle, it is often difficult for them to explain the observed day-to-day and year-to-year variability, let alone to interpret in-situ data from field campaigns. This is mainly because the results from the GCM models in general represent multi-year values averaged over a large area, which is inappropriate for comparisons with observations in a specific time.

Here we introduce the Georgia Tech/Goddard Global Ozone Chemistry Aerosol Radiation and Transport (GOCART) model, which can be potentially the most suitable tool to link the satellite and in-situ obser-

vations. The main advantage of the model, which is also the main difference between this model and the previously published models, is that the GOCART model is driven by the assimilated meteorological fields, which are generated in the Goddard Earth Observing System Data Assimilation System (GEOS DAS). This type of model is therefore appropriate for interpreting measurements for a specific period of time. And because the GOCART model is a global scale model, it is also convenient to use in analyzing satellite data and conducting global assessments.

In this paper, we provide a detailed description of the model components used for simulating the tropospheric sulfur cycle (section 2). The global distributions and 6-year budgets for sulfate and its precursors are presented (section 3), and the anthropogenic contribution to the sulfate burden is discussed (section 5). Results from our model are compared with those from two most recent model studies [Koch *et al.*, 1999; Barth *et al.*, 2000 and Rasch *et al.*, 2000] (section 4 and 5). A detailed evaluation of the model results with observations and budgets for several continental and oceanic regions are presented in a companion paper [Chin *et al.*, this issue]. It is noted that in addition to sulfate, other aerosol components are also simulated in the GOCART model, which include dust (P. Ginoux *et al.*, manuscript in preparation, 2000), carbonaceous, and sea salt aerosols (in progress). With all the major aerosols simulated, we will be able to compare the aerosol properties generated in the model with those retrieved from the satellite measurements, and apply the model to global aerosol analysis.

2. Model Description

2.1. Model Framework

The GOCART model uses the GEOS DAS assimilated meteorological data [Schubert *et al.*, 1993]. The spatial resolution of the model is the same as in the GEOS DAS, which has a horizontal resolution of 2° latitude by 2.5° longitude. The vertical resolution varies with different versions of the GEOS DAS. There are 20 vertical sigma levels in version 1 (GEOS-1, available for the period of January 1980-November 1995), extending from the surface to 10 mb [Allen *et al.*, 1996; Chin *et al.*, 1998]. In version GEOS-1.3 (available from April 1995 to November 1997), designed to support the STRAT (Stratospheric Tracers of Atmospheric Transport) mission, there are 46 vertical levels with approximately 26 of them in the stratosphere and the model top at 0.1 mb. In our tro-

ospheric simulation, we have aggregated the top 23 levels (from 40 mb to 0.1 mb) in the GEOS-1.3 to 3 levels and kept the lowest 23 levels (from surface to 40 mb) as the same resolution as in the GEOS-1.3 such that the total number of model vertical levels is 26. The lowest 5 layers in both GEOS-1 and GEOS-1.3 are centered at approximately 50, 250, 600, 1100, and 1800 meters above the surface. Newer versions of the GEOS DAS data, for example, GEOS-2 and GEOS-3, with higher vertical or horizontal resolutions have become available for the time periods after November 1997.

The GEOS DAS meteorological data contain not only prognostic fields, such as horizontal winds, temperature, and pressure, but also extensive diagnostic fields, such as cloud mass flux, surface precipitation rates, boundary layer height, and surface roughness. Table 1 lists the GEOS DAS archived prognostic and diagnostic fields used in our sulfur simulations.

We present in this paper a 6-year simulation from 1989 to 1994. Four sulfur species are simulated in the model: dimethylsulfide (DMS), SO_2 , sulfate, and methanesulfonic acid (MSA). There are seven modules representing atmospheric processes of these sulfur species: emission, chemistry, advection, convection, diffusion, dry deposition, and wet deposition. The model solves the continuity equation using the method of operator splitting. The model time step is 20 minutes for advection, convection, and diffusion, and 60 minutes for the other processes. The instantaneous meteorological fields in Table 1 are linearly interpolated to the model time. Initialization was done for the last 3 months of 1988, starting from low concentrations (0.1 ppt) for all four sulfur species.

2.2. Transport

The advection and convection schemes used in the model have been described in detail elsewhere [Allen *et al.*, 1996]. Here, briefly, advection is computed by a flux-form semi-Lagrangian method [Lin and Rood, 1996]. Moist convection is parameterized using archived cloud mass flux fields from the GEOS DAS. In the previous model studies using the GEOS DAS fields, the boundary layer mixing was parameterized such that a fixed fraction of material was uniformly mixed within the boundary layer [Allen *et al.*, 1996; Chin *et al.*, 1998]. It was found very difficult to choose a universal value of the mixing fraction since it does not reflect the boundary layer turbulence [Chin *et al.*, 1998]. In the GOCART model, the boundary layer turbulent mixing is computed using

a second-order closure scheme [Helfand and Labraga, 1988], which was also used in the GEOS DAS analysis for heat and moisture turbulent mixing [Takacs *et al.*, 1994]. The scheme takes into account both growing and decaying turbulence. The turbulent diffusion coefficient is a function of the turbulent kinetic energy, the buoyancy and wind shear parameters.

2.3. Sulfur Emissions

The GOCART model includes emissions of DMS from the ocean, SO_2 and sulfate from anthropogenic activities, and SO_2 from biomass burning, aircraft exhaust, and volcanic eruptions. Figure 1 shows an annually averaged emission flux from anthropogenic and natural sources (DMS and volcanic SO_2) for 1990.

Anthropogenic emissions are taken from the Emission Database for Global Atmospheric Research (EDGAR) for the year of 1990 [Olivier *et al.*, 1996]. The annual total emission rate is $72.8 \text{ Tg S yr}^{-1}$ which includes emissions from industrial processes ($59.3 \text{ Tg S yr}^{-1}$), residential and commercial consumptions (8.5 Tg S yr^{-1}), and transportation (road, rail, and shipping, 5.0 Tg S yr^{-1}). The fraction of direct sulfate emission has been estimated from 1.4% to 5% of the total emission [Benkovitz *et al.*, 1996]; we assume here a fraction of 5% for Europe and 3% for elsewhere. The rest is emitted as SO_2 . Emission rates are assumed to be constant throughout the year except for Europe, where a seasonal variation is imposed such that the emission rates are maximum in winter (30% higher than the annual average) and minimum in summer (30% lower than the annual average). This seasonal variation reflects mainly the demand for domestic heating [Sandnes and Styve, 1992].

Emission of DMS from the ocean is calculated as a product of the seawater DMS concentration and sea-to-air transfer velocity. Monthly averaged surface seawater DMS concentrations in $1^\circ \times 1^\circ$ grid resolution are taken from Kettle *et al.* [1999]. This seawater DMS concentration map is generated based on the compilation of a database of over 15,000 measurements around the globe. The transfer velocity of DMS is computed using an empirical formula from Liss and Merlivat [1986], which assumes linear relationships between the transfer velocity and the 10-meter wind speed. Diffusion of DMS within the ocean surface water is taken into account as a function of sea surface temperature [Saltzman *et al.*, 1993]. The 10-m winds used in the model are the remote sensing data from the Special Sensor Microwave Imager (SSM/I) operated on a series of satellites in the Defense Mete-

Figure

orological Satellite Program [Atlas *et al.*, 1996]. The SSM/I winds have been found to represent accurately the local observations [Chin *et al.*, 1998]. It has been noted that there could be a factor of 2 or more differences in the transfer velocity calculated from different formulae [e.g., Smethie *et al.*, 1985; Wanninkhof *et al.*, 1992; Erickson *et al.*, 1993], and a single parameterization of transfer velocity based on wind speed alone is not sufficient to describe DMS flux from the different regions of the oceans [Chin *et al.*, 1998].

Volcanic sources of SO₂ include emissions from both continuously active and sporadically erupting volcanoes. The continuous volcanic emissions are taken from a database of Andres and Kasgnoc [1998]. The database includes SO₂ released from 49 volcanoes which have been continuously active over the last 25 years with an emission rate of 4.8 Tg S yr⁻¹. We assume that SO₂ is injected at a constant rate within 1 km above the crater altitudes. For the sporadically erupting volcanoes, we use the volcanic database from the Smithsonian Global Volcanism Program [Simkin and Siebert, 1994] which has documented the locations, erupting dates and duration, and the volcanic explosivity index (VEI) up to 1994. We then use the VEI to estimate the volcanic cloud height [Simkin and Siebert, 1994], and obtain the amount of SO₂ emitted to the atmosphere by a relationship between VEI and SO₂ flux [Schnetzler *et al.*, 1997]. When they become available, satellite observed volcanic emission data from the Total Ozone Monitoring Spectroscopy (TOMS) instrument [Bluth *et al.*, 1997] are used to replace the calculated emission rates. We further assume that SO₂ is injected within a slab which is located at the top portion of the erupting volcanic cloud with a thickness of 1/3 of the cloud column [L. Glaze, personal communication, 1998]. This assumption is based on the observations of plume height and thickness after eruption [e.g., McCormick *et al.*, 1995] and the results from volcanic plume dispersion models [e.g., Suzuki, 1983].

Other sources of SO₂ in the model include biomass burning (2.3 Tg S yr⁻¹) and aircraft emissions (0.07 Tg S yr⁻¹). Seasonal biomass burning emissions are from Spiro *et al.* [1992]. Aircraft emission is calculated based on the monthly averaged fuel consumption inventory for 1992 from NASA's Atmospheric Effects of Aviation Project (AEAP), assuming an emission index of 1.0, i.e., 1 g SO₂ emitted per kg fuel burned [Weisenstein *et al.*, 1996].

In our 6-year simulation presented in this paper, we have used the same seasonal emissions from an-

thropogenic, biomass burning, aircraft, and continuously active volcanic sources for every year. The only interannually variable sources are the emissions from sporadically erupting volcanoes (based on documented events) and DMS from the ocean (due to the change of surface wind speeds).

2.4. Chemistry

Chemical reactions included in the model are: DMS oxidation by OH during the day to form SO₂ and MSA, and by nitrate radicals (NO₃) at night to form SO₂; SO₂ oxidation by OH in air and by H₂O₂ in cloud to form sulfate. Reaction rates are taken from DeMore *et al.* [1997]. The yields of SO₂ and MSA from DMS+OH reaction are assumed to be the same as in Chin *et al.* [1996], i.e., 100% SO₂ from the abstraction channel, and 75% SO₂ and 25% MSA from the addition channel. We prescribe concentrations of OH, NO₃, and H₂O₂ from the monthly averaged fields generated in the IMAGES model [Müller and Brasseur, 1995]. Figure 2 plots the zonally averaged concentrations of OH and H₂O₂ for January and July. A diurnal variation of OH concentrations is imposed by scaling the average OH fields to the cosine of solar zenith angle. Since the concentrations of NO₃ over the ocean at night are always orders of magnitude higher than those during the day, they are assumed to be zero in the daytime and are evenly distributed over the night.

Because cloud water content is not available in GEOS-1 and GEOS 1.3, we parameterize the in-cloud oxidation of SO₂ by H₂O₂ as a function of cloud fraction, following Chin *et al.* [1996]. Cloud fraction f_c for each grid box is assumed as an empirical function of the relative humidity in that grid box, following Sundqvist *et al.* [1989]:

$$f_c = 1 - \sqrt{1 - \frac{r - r_0}{1 - r_0}}$$

where r is the relative humidity and r_0 is the threshold relative humidity for condensation specified as a function of pressure [Xu and Krueger, 1991]. Within the cloud fraction we assume that the formation of sulfate is determined by the concentration of the limiting reagent, i.e., the lesser amount between SO₂ and H₂O₂. During the chemistry time step (1-hour) H₂O₂ is depleted as the aqueous phase reaction of SO₂+H₂O₂ can be completed in less than one hour [Daum *et al.*, 1984]. The recovery time of H₂O₂ varies considerably in the literature, from instantaneous replenishment to a day in winter [Koch *et al.*, 1999].

Figure 2

Here we assume that H_2O_2 is regenerated to its prescribed value every 3 hours, similar to the time scale used in *Chin et al.* [1996].

2.5. Dry Deposition

Dry deposition velocities for SO_2 , sulfate, and MSA are calculated using the resistance-in-series scheme [Wesely and Hicks, 1977]. In this scheme, dry deposition velocities are determined as a reciprocal of the sum of aerodynamic resistance, sub-layer resistance, and surface resistance. The aerodynamic resistance is taken from the GEOS DAS archive, which is a product of the exchange coefficient for heat and moisture and the surface friction velocity. The sub-layer and surface resistance for SO_2 and sulfate are calculated using the formulation of Walcek et al. [1986] and Wesely [1989]. The dry deposition velocity of MSA is assumed to be the same as that of sulfate. We impose a minimum SO_2 dry deposition velocity of 0.2 cm s^{-1} over the ice and snow and in the polar regions [Voldner et al., 1986; Tarrason and Iversen, 1998]. Typically, the diurnally averaged dry deposition velocity for SO_2 over the land is $0.2\text{-}0.4 \text{ cm s}^{-1}$, but it varies significantly over the ocean, from 0.6 to 0.8 cm s^{-1} under stable conditions to 1 to 2 cm s^{-1} under unstable conditions. For sulfate, a value of $0.08\text{-}0.12 \text{ cm s}^{-1}$ is found over the oceans and $0.1\text{-}0.3$ over the land except at latitudes higher than 60° in the winter season ($0.01\text{-}0.05 \text{ cm s}^{-1}$). These values are in general consistent with the data from limited direct measurements and with other calculated values [e.g., Voldner et al., 1986; Walcek et al., 1986; Ganzeveld et al., 1998 and references therein].

2.6. Wet Scavenging

Wet scavenging of soluble species in the model includes rainout (in-cloud precipitation) and washout (below cloud precipitation) in large-scale precipitation and in deep convective cloud updraft. The GEOS DAS diagnoses the total precipitation at the ground as an column integral of specific humidity change due to moist processes [Takacs et al., 1994]. Here we normalize the precipitation rates from the GEOS DAS to those from an observation based data product, which is a merged dataset combining satellite observations, ground station rain gauge measurements, and the GEOS DAS precipitation fields [P. Houser, manuscript in preparation, 2000; Huffman et al., 1997]. Distribution of large-scale precipitation in a vertical column is estimated based on the specific

humidity changes diagnosed in the GEOS DAS:

$$P_{ls}(k) = c \Delta q_t(k) \frac{Q_{ls}}{Q_t}$$

where $P_{ls}(k)$ is the large-scale precipitation rate at level k , Q_{ls} and Q_t are respectively the column integrated specific humidity change due to large-scale or total (large-scale and convective) moist process. c is the ratio of the precipitation rate in the merged product to that in the GEOS DAS, and $\Delta q_t(k)$ is the total specific humidity change at level k where a negative value indicates a precipitation and a positive value implies an evaporation.

Removal of sulfate and MSA by large-scale rain is calculated as a first-order loss process using parameters of Giorgi and Chameides [1986]. The change of aerosol mixing ratio within a model time step is:

$$\Delta \chi(k) = \chi(k) f(k) (e^{-\beta(k) \Delta t} - 1)$$

where $\chi(k)$ is the mixing ratio at level k , $f(k)$ is the fraction of the grid box experiencing precipitation, $\beta(k)$ is the frequency of cloud to rain conversion, and Δt is the duration of precipitation, which is equal to the wet scavenging time step for large-scale rain. The values of $f(k)$ and $\beta(k)$ are defined by the precipitation amount at each grid box and by a typical liquid water content for large-scale precipitation [Giorgi and Chameides, 1986].

Washout between the cloud layers or below the lowest cloud level is also computed as a first-order loss process, similar to the treatment of rainout. In this case, the fraction of a grid box with precipitation is determined by the largest value of f from the overhead rainy grid box, and β is assumed to be 0.1 mm^{-1} normalized to the precipitation rate [Dana and Hales, 1976]. A fraction of soluble species between or below clouds releases into the grid box if evaporation ($\Delta q_t > 0$) occurs. This fraction is assumed to be the same as that of evaporated water.

It has been found in previous model investigations as well as in field studies that soluble species are scavenged efficiently within the convective cloud updraft [Balkanski et al., 1993; Cohan et al., 1999]. Adapting the principle of Balkanski et al. [1993], we couple the convective scavenging with the moist convection process in our model, and use a scavenging efficiency of 0.4 km^{-1} for soluble aerosol species.

We use the same method for SO_2 wet scavenging as that described in Chin et al. [1996]: we define a soluble fraction of SO_2 as limited by the availability of

H_2O_2 in the precipitating grid box, and scavenge the soluble SO_2 at the same rate as sulfate. When evaporation occurs, a fraction of dissolved SO_2 returns to the grid box as sulfate.

3. Global Budget and Distributions

3.1. Summary of Global Budget

Summary of a 6-year budget of 1989–1994 is presented in Figure 3. Before we discuss the budget, we shall clarify the terms used in our wet removal and aqueous-phase oxidation budgets, since they can sometimes cause confusion. Here, the term “wet scavenging” refers to the loss of a particular tracer in the wet process described in section 2.6 regardless of its transformation within the rain water. With that in mind, we count the amount of SO_2 scavenged and subsequently converted to sulfate in the rain water as a term of wet scavenging of SO_2 , not sulfate. And we do not record this amount as a part of “in-cloud sulfate production” (except for the fraction returned to the atmosphere during the evaporation of raindrops), because the production of sulfate from the dissolved SO_2 in rainwater does not contribute to either the sulfate burden in the atmosphere or the removal of sulfate from the atmosphere. While it seems just a labeling issue for the sulfur budget, counting the wet scavenging of SO_2 as a loss of sulfate can lead to an underestimation of atmospheric sulfate lifetime, since the lifetime is simply the ratio of atmospheric burden to the loss rate.

As shown in Figure 3, the anthropogenic emission is 75 Tg S yr^{-1} , which includes emissions from industrial activities, fuel combustion, ship, and aircraft, as well as from biomass burning. Biogenic emission of DMS from the ocean varies from 13.3 to $15.0 \text{ Tg S yr}^{-1}$, reflecting the changes in the surface wind speeds. Volcanic emissions are also fairly constant from year to year (5.4 – 6.0 Tg S yr^{-1}), except 1991 when a major volcanic eruption of Mt. Pinatubo occurred in June, injecting about 10 Tg S (or 20 Mton SO_2) into the atmosphere. Total volcanic emission for 1991 is $19.6 \text{ Tg S yr}^{-1}$. In a normal year (e.g., without major volcanic eruptions), the fraction of sulfur emitted from natural sources (biogenic and volcanic) is about 20% of the total emission of 94 Tg S yr^{-1} .

In-cloud oxidation of SO_2 is responsible for about 64% of total sulfate production in a normal year, while in-air oxidation accounts for the rest 36%. In contrast, less than half of the sulfate production in 1991 takes place in-cloud, because the Pinatubo eruption

injects most SO_2 into the stratosphere where the gas-phase reaction with OH is the only mechanism in the model to convert SO_2 to sulfate. Dry deposition and wet scavenging remove roughly the same amount of sulfur from the atmosphere (45 – 55 Tg S yr^{-1}). While dry deposition is the most important loss of SO_2 (45%) followed by in-cloud oxidation (27%), wet scavenging eliminates 90% of sulfate produced in the atmosphere. The lifetime is 1.8 days for SO_2 and 5.8 days for sulfate in a normal year.

The annually averaged atmospheric burden for SO_2 is 0.42 – 0.48 Tg S except 1991. The SO_2 burden is 1.6 Tg S in 1991, with most of it residing in the stratosphere, i.e., above 100 – 120 mb in the model (Figure 3). While SO_2 returns to its normal level rather quickly after the Pinatubo eruption (e-folding time about 1 month), it takes much longer for sulfate to relax back to its normal level. As illustrated in Figure 3, three years after the Pinatubo eruption, total sulfate burden in 1994 (0.98 Tg S) is still significantly higher than its pre-Pinatubo value in 1989–1990 (0.63 Tg S).

The only removal process for DMS is its oxidation in the atmosphere. Globally, nearly 90% of DMS emitted from the ocean is oxidized by OH during the day; only 10% is lost at night via reaction with NO_3 . The stable products from DMS oxidation are 89% SO_2 , which can be further oxidized to sulfate, and 11% MSA, which is removed by wet (91%) and dry (9%) depositions. The atmospheric burden for DMS is 0.072 – 0.080 Tg S , and that for MSA is 0.027 – 0.032 Tg S . The lifetime is 1.9–2.2 days for DMS and 6.8–7.2 days for MSA.

We define a term of the sulfate production efficiency as the amount of sulfate produced relative to the total amount of SO_2 emitted and produced in the atmosphere. The sulfate production efficiency is a direct measure of the effectiveness of SO_2 oxidation versus the dry and wet removal of SO_2 . We find in our model a typical production efficiency value of 0.41 – 0.42 , which indicates that only less than half of the SO_2 contributes to sulfate production in the atmosphere, and the rest is mainly deposited to the surface. In the Pinatubo eruption year of 1991, however, the sulfate production efficiency increases to 0.49 , reflecting that the SO_2 released at high altitudes produces sulfate much more effectively than that emitted near the surface.

3.2. Global Distributions

To present some general features simulated in the model, we plot in Figure 4 global distributions of SO₂, sulfate, DMS, and MSA at the surface (Figure 4a) and at 500 mb (Figure 4b) for the pre-Pinatubo year of 1990. Concentrations shown in Figure 4 are average values for 2 seasons: December, January, February (DJF), and June, July, August (JJA). High surface concentrations of SO₂ and sulfate are found in regions of high anthropogenic emissions for both seasons, as expected. The major contrast between DJF and JJA is the strong advection of pollutants from the mid-latitude source regions to the Arctic circle in DJF. While SO₂ concentrations are higher in the winter than in the summer, the reverse is true for sulfate, because of the seasonal variation of SO₂ oxidation rates. Globally, the sulfate production efficiency in January is only 0.27 whereas in July it is 0.48 in 1990.

The distribution of DMS at the surface closely resembles that in seawater. Very high surface air concentrations of DMS (500–2000 ppt) are produced in the model near 60° latitude in the summer hemisphere. These elevated concentrations are directly related to the high DMS emission flux (10–50 $\mu\text{mol m}^{-2} \text{ day}^{-1}$), a product of very high seawater DMS concentrations and strong surface winds. While the surface DMS concentrations at these latitudes in summer seem too high compared with some measurements near the Antarctic coast (< 800 ppt, *Staubes and Georgii*, 1993; *Berresheim et al.*, 1998), the model calculated concentrations of the DMS oxidation products, sulfate and MSA, at high latitude sites (e.g., Palmer Station and Mawson in Antarctica, and Haemey in Iceland) agree with the observations to within 40% [*Chin et al.*, this issue]. This apparent inconsistency needs to be further investigated. Finally, as expected, MSA surface distribution is similar to that of DMS.

One common feature for all sulfur species at 500 mb (Figure 4b) is that they are better mixed zonally and the concentrations are 1 to 2 magnitudes lower than that at the surface, reflecting their relatively short lifetimes (several days). DMS concentrations at 500 mb are higher in the winter hemisphere than in the summer hemisphere, opposite to the pattern found at the surface. This is because the slow oxidation rates of DMS in winter allow DMS to be transported to higher altitudes. On the other hand, the DMS loss rates are higher in summer than in winter due to the higher OH concentrations: thus only a small fraction of DMS escapes from the boundary

layer in summer despite the higher emission rates.

The annually averaged zonal mean distributions of SO₂, sulfate, DMS, and MSA for 1990 are shown in Figure 5. As expected, both SO₂ and sulfate exhibit high concentrations in the northern hemisphere. In the tropics, DMS is pumped to the upper troposphere by the deep convective process. Interestingly, the same process is also responsible for the low sulfate concentration in the middle to upper troposphere over the tropics, thanks to the efficient wet scavenging of sulfate in cloud convection. This feature also appeared in the model simulations of *Feichter et al.* [1996] and *Koch et al.* [1999], but was lacking in some other models (e.g., *Chin et al.*, 1996; *Barth et al.*, 1999), depending on the convective process in the meteorological data and the efficiency of in-cloud scavenging in different models.

We plot in Figure 6 the column total sulfate sources and sinks in the 1990 simulation as a function of latitude. It can be seen that in-cloud oxidation of SO₂ is the most important source of sulfate, especially at high latitudes (60°N and higher in the northern hemisphere, and between 40°S and 70°S in the southern hemisphere), where in-cloud oxidation contributes 80–90% of the total sulfate source. While scavenging by large-scale rain dominates the sulfate loss over mid- and high latitudes, wet convective scavenging dominates over the tropics and subtropics. Dry deposition in general accounts for less than 20% of sulfate loss at all latitudes except in the polar regions.

4. Comparisons with Other Global Model Studies

We focus here on the comparison of sulfur budget in the GOCART model simulation for 1990 with two of the most recent global model studies: *Koch et al.* [1999], using the Goddard Institute for Space Studies' general circulation model version II' (GISS GCM), and *Barth et al.* [2000] and *Rasch et al.* [2000], using the NCAR Community Climate Model (NCAR CCM3). Intercomparisons involving other earlier models (e.g., *Langner and Rodhe*, 1991; *Pham et al.*, 1995; *Feichter et al.*, 1996; *Chin et al.*, 1996) have been presented in previous model studies [*Chin et al.*, 1996; *Koch et al.*, 1999; *Rasch et al.*, 2000] and will not be discussed in detail here. We will only summarize the major differences between this study and an earlier work [*Chin et al.*, 1996].

Table 2 summarizes the comparison of sulfur budgets among the GOCART, GISS, and NCAR mod-

Figure

Figure

Table

els. Our total emission ($93.9 \text{ Tg S yr}^{-1}$) is higher than that in both GISS and NCAR models (83 Tg S yr^{-1}). This is because we use the EDGAR database of 1990 emission inventory ($72.8 \text{ Tg S yr}^{-1}$) which also includes emissions from shipping and landuse, while the GISS and NCAR models use the GEIA emission inventory (67 Tg S yr^{-1}) for the 1985 emission scenario [Benkovitz *et al.*, 1996]. The biomass burning emission in our model is the same as that in the GISS model (2.3 Tg S yr^{-1}), but the volcanic emission (5.5 Tg S yr^{-1}) is much higher than that in the GISS model (3.5 Tg S yr^{-1}), because we include emissions from both continuously active and sporadically erupting volcanoes, while Koch *et al.* [1999] considers only non-eruptive volcanoes. Volcanic and biomass burning emissions are not included in the NCAR model. Emission of DMS calculated in our model is $13.3 \text{ Tg S yr}^{-1}$ for 1990, about 30% higher than that in the GISS model ($10.7 \text{ Tg S yr}^{-1}$), even though both models use the same formula for transfer velocity and the same DMS seawater concentrations in calculating DMS emission rates. This difference may be attributed to the lower 10-meter wind speeds in the GISS GCM. The NCAR model calculates a total DMS emission of $15.5 \text{ Tg S yr}^{-1}$, based on the latitudinal bands of DMS flux in Bates *et al.* [1992] and the distribution of the ocean color in the remote sensing products.

Our model estimates an equal amount of sulfur being removed by dry deposition and wet scavenging (50% for each process), while a slightly higher fraction of dry deposition (54% dry, 46% wet) is obtained in the GISS model and the wet removal is about twice as effective as dry deposition in the NCAR model.

Total sulfate production from SO_2 oxidation is $38.5 \text{ Tg S yr}^{-1}$ in our model. Although this value is the lowest among the three models, remember that we do not count the SO_2 loss in wet scavenging as a part of sulfate production while both the GISS and NCAR models do. As we stated in the previous section, even though the amount of SO_2 scavenged by the rain is subsequently converted to sulfate in rainwater, this process does not play a role in determining the atmospheric sulfate concentration or removal; we thus consider the in-rain sulfate production as ineffective. Should we include the SO_2 wet scavenging as a part of sulfate production, the value would be $49.1 \text{ Tg S yr}^{-1}$ which is between the GISS and NCAR model.

As we have shown in the previous section, 89% of the DMS emitted from the ocean produces SO_2 ($11.9 \text{ Tg S yr}^{-1}$). Of this amount, 87% is produced

via $\text{DMS} + \text{OH}$ and 13% via $\text{DMS} + \text{NO}_3$. The SO_2 production is more efficient in the GISS model (93%), whereas the NCAR model assumes SO_2 as the only DMS oxidation product.

The GISS model has the highest SO_2 and sulfate burden among the three models, which was attributed to the use of prognostic H_2O_2 and an insufficient entrainment of H_2O_2 from the cloud base to oxidize SO_2 in highly polluted regions [Koch *et al.*, 1999]. On the other hand, the NCAR model also uses prognostic H_2O_2 but shows the lowest SO_2 and sulfate burden. The cause of the discrepancy is likely a combination of the differences in cloud processing, oxidant concentrations, precipitation rates, among others, between the models. The DMS burden and lifetime in our model is 22% and 41% higher than those in the NCAR model, even though both models have used the same prescribed OH and NO_3 fields for DMS oxidation. Possible explanations include the difference in DMS emission rates, which are higher in our model at high latitudes where DMS oxidation is slower. The lifetime of DMS in the GISS model is very close to that in our model, although the DMS burden is lower in the GISS model, probably due to the lower emission rates.

The lifetime of 2.6 days for SO_2 in the GISS model is about 40% longer than the ones in both our model (1.8 days) and the NCAR model (1.9 days), reflecting a slower removal rate in the GISS model. Regarding the lifetime of sulfate, we estimate a value of 5.8 days with respect to the sulfate dry deposition and wet scavenging. If we had included the amount of SO_2 lost by wet scavenging as a sink of sulfate, as the GISS and NCAR models have, then the sulfate lifetime in our model would be 4.6 days, which is lower than the GISS model but higher than the NCAR model. The point we try to make here is that the atmospheric sulfate residence time is underestimated when wet scavenging of SO_2 is included as a loss term of sulfate. The lifetime of DMS is similar to that in the GISS model but higher than that in the NCAR model, whereas the lifetime of MSA is slightly lower than that in the GISS model (MSA is not simulated in the NCAR model).

To examine the differences between the models in loss rates for individual sinks, we list in Table 2 the loss frequencies for each process, defined as the SO_2 or sulfate atmospheric burden divided by their individual removal rates. While dry removal processes for SO_2 (dry deposition and in-air oxidation) are the most efficient in our model, wet processes (aqueous

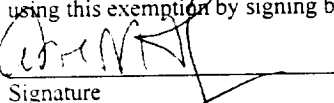
GSFC STI PUBLIC DISCLOSURE EXPORT CONTROL CHECKLIST

The Export Control Office requests your assistance in assuring that your proposed disclosure of NASA scientific and technical information (STI) complies with the Export Administration Regulations (EAR, 15 CFR 730-774) and the International Traffic In Arms Regulations (ITAR, 22 CFR 120-130). The NASA Export Control Program requires that every domestic and international presentation/publication of GSFC STI be reviewed through the GSFC Export Control Office in accordance with the NASA Form 1676 NASA Scientific and Technical Document Availability Authorization (DAA) process. Release of NASA information into a public forum may provide countries with interests adverse to the United States with access to NASA technology. Failure to comply with the ITAR regulations and/or the Commerce Department regulations may subject you to fines of up to \$1 million and/or up to ten years imprisonment per violation. Completion of this checklist should minimize delays in approving most requests for presentation/publication of NASA STI.

Generally, the export of information pertaining to the design, development, production, manufacture, assembly, operation, repair, testing, maintenance or modification of defense articles, *i.e.*, space flight hardware, ground tracking systems, launch vehicles to include sounding rockets and meteorological rockets, radiation hardened hardware and associated hardware and engineering units for these items are controlled by the State Department under the ITAR. A complete listing of items covered by the ITAR can be accessed at <http://gsfc-blusun.gsfc.nasa.gov/export/regsitar.htm>. The export of information with respect to ground based sensors, detectors, high-speed computers, and national security and missile technology items are controlled by the U.S. Commerce Department under the EAR. If the information intended for release falls within the above categories but otherwise fits into one or more of the following exemptions, the information may be released.

EXEMPTION I

If your information is already in the public domain in its entirety through a non-NASA medium and/or through NASA release previously approved by the Export Control Office, the information is exempt from further review. If the information falls into this category, you may attest that you are using this exemption by signing below.

 23 Aug 2000
Signature Date

EXEMPTION II

If your information pertains exclusively to the release of scientific data, *i.e.* data pertaining to studies of clouds, soil, vegetation, oceans, and planets, without the disclosure of information pertaining to articles controlled by the ITAR or EAR, such as flight instruments, high speed computers, or launch vehicles, the information is exempt from further review. If the information falls into this category, you may attest that you are using this exemption by signing below.

Signature Date

EXEMPTION III

If your information falls into the areas of concern as referenced above, but is offered at a general purpose or high level, *i.e.* poster briefs and overviews, where no specific information pertaining to ITAR or EAR controlled items is offered, the information is exempt from further review. If the information falls into this category, you may attest that you are using this exemption by signing below.

Signature Date

EXEMPTION IV

If your information is not satisfied by the 3 exemptions stated above, the information may be released using exemption 125.4(b)(13) of the ITAR. Use of this exemption is afforded only to agencies of the Federal Government and allows the release of ITAR controlled information into the public domain. But the GSFC Export Control Office has determined that use of this exemption will be allowed only after we receive assurance that such release is a responsible action. To this end, an internal guideline has been established pursuant to the use of this exemption: That the information does not offer specific insight into design, design methodology, or design processes of an identified ITAR controlled item in sufficient detail (by itself or in conjunction with other publications) to allow a potential adversary to replicate, exploit and/or defeat controlled U.S. technologies. All signatures of approval on NASA Form 1676 expressly indicate concurrence with the responsible use of Exemption IV when Exemption IV has been cited by the author. If you determine that you have met this criteria, you may attest your determination by signing below, and the GSFC Export Control Office will offer favorable consideration toward approving your presentation/publication request under this special exemption.

Signature Date

If you do not satisfy the above exemptions, please contact the GSFC Export Control Office for further clarification on the releasability of your information under the ITAR or EAR.



National Aeronautics
and Space
Administration

NASA Scientific and Technical Document Availability Authorization (DAA)

The DAA approval process applies to all forms of published NASA Scientific and Technical Information (STI), whether disseminated in print or electronically. It is to be initiated by the responsible NASA Project Officer, Technical Monitor, author or other appropriate NASA official for all presentations, reports, papers, and proceedings that contain NASA STI Explanations are on the back of this form and are presented in greater detail in NPG 2200.2, "Guidelines for Documentation, Approval, and Dissemination of NASA Scientific and Technical Information."

- ☐ Original
☐ Modified

I. DOCUMENT/PROJECT IDENTIFICATION

TITLE

Atmospheric Sulfur Cycle Simulated in
the Global Model GOCART: Model
Description and Global Properties

AUTHOR (S)

M. Chin
R. B. Rood
S.-J. Lin
J.-F. Muller
A. M. Thompson

ORIGINATING NASA ORGANIZATION

NASA Goddard Space Flight Center

PERFORMING ORGANIZATION (if different)

Atmospheric Chemistry & Dynamics Branch

CONTRACT/GRANT/INTERAGENCY/PROJECT NUMBER(S)

DOCUMENT NUMBER(S)

DOCUMENT DATE

For presentations, documents, or other STI to be externally published (including through electronic media), enter appropriate information on the intended publication such as name, place, and date of conference, periodical or journal name, or book title and publisher in the next box. These documents must be routed to the NASA Headquarters or Center Export Control Administrator for Approval (see Sections III and VIII).



J. Geophys. Res.

II. SECURITY CLASSIFICATION

CHECK ONE (One of the five boxes denoting Security Classification must be checked.)

☐ SECRET ☐ SECRET RD ☐ CONFIDENTIAL ☐ CONFIDENTIAL RD ☒ UNCLASSIFIED

III. AVAILABILITY CATEGORY

☐ ITAR ☐ EAR

Export Controlled Document - USML Category /CCL Export Control
Classification Number (ECCN) (Documents marked in this block must have the
concurrence/approval of the NASA Headquarters or Export Control Administrator (see Section VIII).

☐ TRADE SECRET
☐ SBIR
☐ COPYRIGHTED

Confidential Commercial Document (check appropriate box at left and indicate below the appropriate
limitation and expiration:

- ☐ U.S. Government agencies and U.S. Government agency contractors only
☐ NASA contractors and U.S. Government only
☐ U.S. Government agencies only
☐ NASA personnel and NASA contractors only
☐ NASA personnel only
☐ Available only with the approval of issuing office
☐ Limited until (date)

☒ PUBLICLY
AVAILABLE

Publicly available documents must be unclassified, may not be export controlled, may not contain trade secret or
confidential commercial data, and should have cleared any applicable patents application process.

IV. DOCUMENT DISCLOSING AN INVENTION

THIS DOCUMENT MAY BE RELEASED ON
(date)

NASA HQ OR CENTER PATENT OR INTELLECTUAL PROPERTY COUNSEL SIGNATURE

DATE

V. BLANKET RELEASE (OPTIONAL)

- ☐ All documents issued under the following contract/grant/project number
may be processed as checked in Sections II and III.
☐ The blanket release authorization granted on (date)
☐ is RESCINDED - Future documents must have individual availability authorizations.
☐ is MODIFIED - Limitations for all documents processed in the STI system under the blanket release should be
changed to conform to blocks as checked in Sections II and III.

VI. AUTHOR/ORIGINATOR VERIFICATION			
I HAVE DETERMINED THAT THIS PUBLICATION:			
<input type="checkbox"/> DOES contain export controlled, confidential commercial information, and/or discloses an invention for which a patent has been applied, and the appropriate limitation is checked in Sections III and/or IV.			
<input type="checkbox"/> does NOT contain export controlled, confidential commercial information, nor does it disclose an invention for which a patent has been applied, and may be released as indicated above.			
NAME OF AUTHOR/ORIGINATOR	MAIL CODE	SIGNATURE	DATE
Anne Thompson	916	<i>[Signature]</i>	2/9/2000
VII. PROJECT OFFICER/TECHNICAL MONITOR/DIVISION CHIEF REVIEW			
<input checked="" type="checkbox"/> APPROVED FOR DISTRIBUTION AS MARKED ON REVERSE <input type="checkbox"/> NOT APPROVED			
NAME OF PROJECT OFFICER OR TECH. MONITOR	MAIL CODE	SIGNATURE	DATE
Franco Einaudi	910	<i>[Signature]</i>	8/28/00
VIII. EXPORT CONTROL REVIEW/CONFIRMATION			
<input checked="" type="checkbox"/> Public release is approved <input checked="" type="checkbox"/> Export controlled limitation is not applicable			
<input type="checkbox"/> Export controlled limitation is approved <input type="checkbox"/> Export controlled limitation (ITAR/EAR) marked in Section III is assigned to this document			
USML CATEGORY NUMBER	CCL ECCN NUMBER	HQ OR CENTER EXPORT CONTROL ADMINISTRATOR (as applicable)	DATE
N/A	N/A	J. R. Hedgpeth	8/16/2000
IX. PROGRAM OFFICE OR DELEGATED AUTHORITY REVIEW			
<input checked="" type="checkbox"/> APPROVED FOR DISTRIBUTION AS MARKED ON REVERSE <input type="checkbox"/> NOT APPROVED			
NAME OF PROGRAM OFFICE REPRESENTATIVE	MAIL CODE	SIGNATURE	DATE
Vincent V. Salomonson	900	<i>[Signature]</i>	7/31/00
X. DISPOSITION			
THIS FORM WHEN COMPLETED, IS TO BE SENT TO YOUR CENTER PUBLICATIONS OFFICE			

INSTRUCTIONS FOR COMPLETING THE NASA SCIENTIFIC AND TECHNICAL DOCUMENT AVAILABILITY AUTHORIZATION (DAA) FORM

Purpose. This DAA form is used to prescribe the availability and distribution of all NASA-generated and NASA-funded documents containing scientific and technical information (including those distributed via electronic media such as the World Wide Web and CD-ROM).

Requirements. The author/originator must provide either a suitable summary description (title, abstract, etc.) or a completed copy of the document with this form. This form is initiated by the document author/originator and that individual is responsible for recommending/determining the availability/distribution of the document. The author/originator completes sections I through III, and VI. The author/originator is also responsible for obtaining information and signature in Section IV to the extent the document discloses an invention for which patent protection has been applied. Subsequent to completion of these sections, the author/originator forwards the document to the appropriate Project Manager/Technical Monitor/Division Chief for further review and approval in Section VII, including a re-review of the planned availability and distribution. Once this approval is obtained, the DAA is forwarded to the NASA Headquarters or Center Export Administrator for completion of Section VIII. It is then forwarded for completion of Section IX to the cognizant NASA Headquarters Program Office or Delegated Authority, who provides final review and approval for release of the document as marked.

When to Use This Form. Documents containing STI and intended for presentation or publication (including via electronic media) must be approved in accordance with the NASA STI Procedures and Guidelines (NPG 2200.2). Documents that are to be published in the NASA STI Report Series must be coordinated with the appropriate NASA Headquarters or Center Scientific and Technical Information Office in accordance with NPG 2200.2. Note that information on the Report Documentation Page (if attached) is not to be entered on the DAA except for title, document date, and contract number.

How to Use this Form. Specific guidelines for each section of this form are detailed below:

I. Document/Project Identification. Provide the information requested. If the document is classified, provide instead the security classification of the title and abstract. (Classified information must not be entered on this form). Include RTOP numbers on the Contract/Grant/Interagency/Project Number(s) line. Provide information on presentations or externally published documents as applicable.

II. Security/Classification. Enter the applicable security classification for the document. Documents, if classified, will be available only to appropriately cleared personnel having a "need to know."

III. Availability Category for Unclassified Documents. Check the appropriate category or categories.

Export Controlled Document. If the document is subject to export restrictions (see NPG 2200.2, paragraph 4.5.3), the appropriate restriction must be checked, either International Traffic in Arms Regulations (ITAR) or Export Administration Regulations (EAR), and the appropriate United States Munitions List (USML) category or Commerce Control List (CCL). Export Control Classification Number (ECCN) must be cited.

Confidential Commercial Documents (Documents containing Trade Secrets, SBIR documents, and/or Copyrighted Information). Check the applicable box (see NPG 2200.2 paragraph 4.5.7). When any of these boxes are checked, also indicate the appropriate limitation and expiration in the list to the right of these restrictions. These limitations refer to the user groups authorized to obtain the document. The limitations apply to both to the initial distribution of the documents and the handling of requests for the documents. The limitations will appear on and apply to reproduced copies of the document. Documents limited to NASA personnel should not be made available to onsite contractors. If the Available Only With the Approval of Issuing Office Limitation is checked, the NASA Center for Aerospace Information will provide only bibliographic processing and no initial distribution; CASI will refer all document requests to the issuing office.

Publicly Available Document - Unrestricted Distribution. Check this box if the information in the document may be made available to the general public without restrictions (unrestricted domestic and international distribution). If the document is copyrighted (see paragraph 4.5.7.3 in NPG 2200.2), also check the "Copyrighted" box in this section.

IV. Document Disclosing an Invention. This must be completed when the document contains information that discloses an invention (see NPG 2200.2, paragraph 4.5.9). When this box is checked, an additional appropriate availability category must be checked. Use of this category must be approved by NASA Headquarters or Center Patent Counsel or the Intellectual Property Counsel.

V. Blanket Release (Optional). Complete this optional section whenever subsequent documents produced under the contract, grant, or project are to be given the same distribution and/or availability as described in Sections II and III. More than one contract number or RTOP Number can be entered. This section may also be used to rescind or modify an earlier Blanket Release. All blanket releases must be approved by the Program Office or its designee and concurred with by the Office of Management Systems and Facilities.

VI. Author/Originator Verification. Required for all DAA forms.

VII. Project Officer/Technical Monitor/Division Chief Review. The Project Officer/Technical Monitor/Author or Originator Division Chief or above must sign and date the form. The office code and typed name should be entered.

VIII. Export Control Review/Confirmation. This section is to be completed by the authorized NASA Headquarters or Center Export Control Administrator for all documents.

IX. Program Office or Delegated Authority Review. This section is to be completed by the duly authorized official representing the NASA Headquarters Program Office. Any delegation from NASA Headquarters to a NASA Center in accordance with NPG 2200.2 should be entered here.

X. Disposition. For NASA Center use

phase production and wet removal) are the most effective in the NCAR model but the least effective in the GISS model. The effectiveness of the wet process is almost inversely proportional to the SO_2 and sulfate burden, which are the lowest in the NCAR model and highest in the GISS model. For example, a ratio of the sulfate burden between the GOCART, GISS, and NCAR models are 1:1.3:0.9, that of the SO_2 burden is 1:1.2:0.9, which is also the ratio of the inverse of the total sulfur wet deposition rate. Interestingly, the sulfate burden is also inversely proportional to the wet production rate of sulfate (in-cloud and in-rain); a ratio of 1:1.1:0.9 is found between the three models. These linear relations clearly confirm the importance of the wet processes in determining the sulfur burden in the atmosphere. Therefore, emphasis should be given to improving the wet physical and chemical processes and validating the parameters used in modeling these processes, such as cloud distribution, cloud fractions, precipitation amount, scavenging efficiencies, and the aqueous phase oxidation rates.

Comparing our zonally averaged concentrations of SO_2 , sulfate, and DMS in Figure 5 with those reported in Koch *et al.* [1999] and Barth *et al.* [2000], we find that the SO_2 concentrations in the GISS model are significantly higher than that in both the NCAR and our model in the lower troposphere. For example, a 500 ppt SO_2 contour in the GISS model reached 700 mb and extended from 27°N to 75°N , while this contour line is confined below 850 mb and at the latitudes between 25°N and 60°N in both the NCAR and our models. A similar difference in sulfate distribution is also found. Our extratropical DMS zonal distribution resembles that in the GISS model with a symmetric distribution between the northern and southern hemispheres. However, in the tropical upper troposphere, there is a second maximum of DMS in our model with a concentration of 5–10 ppt, a feature which is very similar to the NCAR model but not obvious in the GISS model.

The results from the GOCART model differ from that in Chin *et al.* [1996] (using the Harvard/GISS GCM II model) in a number of ways. The major difference is in the sulfate vertical distributions. The zonally averaged sulfate distribution in Figure 5 shows a much less vertical gradient than that in Chin *et al.* [1996]. The difference is attributed mainly to a much more efficient wet scavenging in Chin *et al.* [1996], partly due to the excessive wet convection over some regions, and partly due to the higher wet scavenging efficiency (100% in deep wet convection).

The other difference is in DMS oxidation. Chin *et al.* [1996] found that an oxidant in addition to OH and NO_3 was needed for DMS oxidation in order to reproduce both DMS and sulfate concentrations observed over the remote ocean surface. We do not invoke such an oxidant in this study, and our simulated concentrations for all sulfur species are overall consistent with the observations over the oceans [Chin *et al.*, this issue]. We attribute this difference to the better parameters in calculating the DMS emission rates and the higher (a factor of 2 to 3) OH concentrations over the ocean surface (a factor of 2 to 3) used in this study than those used in Chin *et al.* [1996].

5. Anthropogenic Contributions

We have conducted a model simulation for 1990 without anthropogenic emissions in order to estimate the relative importance of natural and anthropogenic sources to the atmospheric sulfate loading. The total emission for this case is $18.8 \text{ Tg S yr}^{-1}$, which includes only the DMS and volcanic SO_2 sources. The annually averaged column sulfate burden and the anthropogenic contributions for 1990 are shown in Figure 7. The anthropogenic fraction of sulfate is more than 60% in the northern hemisphere, with more than 80% over the United States and the Eurasian continent. A more widely spread anthropogenic influence over the northern hemisphere is found in the GISS [Koch *et al.*, 1999] and NCAR [Rasch *et al.*, 2000] models, with more than 80% anthropogenic sulfate over the entire area at latitudes north of 10°N . In the southern hemisphere, the anthropogenic fraction is generally 20–40% over the ocean in our model (Figure 8), similar to the GISS and NCAR models.

We find that anthropogenic sources contribute to 67% of the total sulfate burden in 1990, a fraction which is somewhat lower than the anthropogenic sulfur emission fraction of 80%. Figure 8 shows the percentage of zonally averaged anthropogenic contribution for two seasons, DJF and JJA, in 1990. As can be seen in Figure 3, the anthropogenic sulfate dominates the sulfate burdens in the northern hemisphere but with distinct patterns between DJF and JJA. It disperses horizontally in DJF with the 80% contourline stretched out to the northern polar region but confined below 600 mb. By contrast, the anthropogenic sulfate is well mixed vertically by the frequent convective activities in JJA with the 80% contour line extended to the tropopause. Of interest is that the anthropogenic contribution increases

Figur

Figur

with the altitude over the mid- to high latitude in the southern hemisphere, resulting from the interhemispheric transport from the northern hemisphere and the convective transport from the mid-latitudes.

When comparing the natural sulfur budget with that in the GISS model [Koch *et al.*, 1999], a major disagreement lies in the lifetimes of SO₂ and sulfate. While in the GISS model the SO₂ lifetime from a natural-source-only run (1.8 days) was shorter than that from a full run (2.6 days), we find that the reverse is the case in our model: 2.4 days in the natural-source-only run and 1.8 days in the full run. As for sulfate, the lifetime stayed the same in both natural and full simulations in the GISS model, but in our model it is longer from the natural simulation (7.2 days) than that from the full simulation (5.8 days). It is expected that SO₂ and sulfate of natural origin should have a longer lifetime than the anthropogenic ones, because they are not as concentrated near the surface, thus not subject to the fast removal by dry and wet depositions.

The anthropogenic contribution to the atmospheric sulfate burden from this study, as well as from the GISS and NCAR models, is significantly higher than that reported by Chin and Jacob [1996]. The latter study found that the anthropogenic sources contributed to only 37% of the sulfate burden, although they accounted for 70% of the total sulfur emission. This is due to the high sulfate production rates from DMS oxidation and more excessive wet scavenging near the mid-latitude continents in Chin *et al.* [1996] than those in this study.

6. Conclusions

We have used the GOCART model to simulate the tropospheric sulfur cycle. The model uses the assimilated meteorological fields from the GEOS DAS, making it potentially the best tool to link the satellite and in-situ observations for global analysis. We have incorporated in the model the most updated emission inventories of anthropogenic, biogenic, and volcanic sources for DMS and SO₂. In a typical year without major volcanic eruptions, we estimate that about 20% of the sulfate precursor emission is from natural sources (biogenic and volcanic) while 80% is anthropogenic. In-air and in-cloud oxidation of SO₂ account for 36% and 64% respectively of the atmospheric sulfate production. We have estimated a sulfate production efficiency as a ratio of the amount of sulfate produced to the total amount of SO₂ emitted and pro-

duced in the atmosphere. A typical production efficiency value of 0.41–0.42 is found, indicating that generally more than half of the SO₂ entering the atmosphere does not contribute to the sulfate production but is either removed by dry deposition or scavenged by the rain. We have reported that in 1990 the atmospheric burdens for SO₂, sulfate, DMS, and MSA are 0.43, 0.63, 0.073, and 0.028 Tg S, respectively, with the corresponding lifetimes of 1.8, 5.8, 2.0, and 7.1 days.

The anthropogenic contribution to the atmospheric sulfate burden is estimated at 67% for 1990, a fraction which is somewhat smaller than that of anthropogenic emission (80%). While it is horizontally spreading out to the northern polar region in DJF, the anthropogenic contribution is vertically well mixed in JJA, with the 80% contour line extended to the tropopause over the mid-latitudes in the northern hemisphere. We have also shown that major volcanic eruptions can significantly change the sulfate formation pathways, distributions, abundance, and lifetime. These effects are seen in our model simulations from 1989 to 1994, a period which includes the major volcanic eruption of Mt. Pinatubo in 1991. It has been demonstrated that while SO₂ returns to its normal level in only a few months after the Pinatubo eruption, it takes several years for sulfate to relax back to its normal atmospheric loading.

Our model results of 1990 have been compared with two most recent model studies, namely the GISS model [Koch *et al.*, 1999] and the NCAR model [Barth *et al.*, 2000; Rasch *et al.*, 2000]. While the annual DMS burden in our model is 20–30% larger than the other two models, our SO₂ and sulfate burdens are lower than those in the GISS model but higher than those in the NCAR model. The relative abundance of the SO₂ and sulfate burden is almost inversely proportional to the rate of wet removal and the rate of wet production of sulfate. This proportionality shows the magnitude of the wet processes in controlling the atmospheric sulfur burden. Therefore, the first priority in future research should be to reduce the large uncertainties associated with the wet physical and chemical processes.

Acknowledgments. We would like to thank Daniel Jacob of Harvard University for many helpful discussions and his comments on this manuscript. We thank Andrea Molod of GSFC for helping with the GEOS data, Joe Ardizzone of GSFC for providing the SSM/I winds, Paul Houser of GSFC for providing the merged precipitation products, Paul Ginoux of Georgia Tech/GSFC for obtain-

ing the GEOS turbulent coefficients, Lee Siebert and Tom Simkin of Smithsonian Institution Global Volcanism Program for providing chronological volcanic eruption data, Lori Glaze and Arlin Krueger of GSFC for discussions of volcanic emissions, Ulrike Lohmann of Dalhousie University for providing cloud fraction formula, and the EDGAR database for providing 1990 SO₂ emission inventory. This research is sponsored by the NASA Atmospheric Chemistry Model and Analysis Program, Global Aerosol Climatology Program, EOS/Interdisciplinary Science Program, Goddard Space Flight Center, and NOAA Aerosol Program.

References

- Allen, D. J., P. Kasibhatla, A. M. Thompson, R. B. Rood, B. G. Doddridge, K. E. Pickering, R. D. Hudson, and S.-J. Lin, Transport-induced interannual variability of carbon monoxide determined using a chemistry and transport model, *J. Geophys. Res.*, **101**, 28,655-28,669, 1996.
- Andres, R. J., and A. D. Kasgnoc, A time-averaged inventory of subaerial volcanic sulfur emissions, *J. Geophys. Res.*, **103**, 25,251-25,261, 1998.
- Atlas, R., R. N. Hoffman, S. C. Bloom, J. C. Jusem, and J. Ardizzone, A multiyear global surface wind velocity dataset using SSM/I wind observations, *Bull. Amer. Meteorol. Soc.*, **77**, 869-882, 1996.
- Balkanski, Y. J., D. J. Jacob, G. M. Gardner, W. C. Graustein, and K. K. Turekian, Transport and residence times of tropospheric aerosols inferred from a global three-dimensional simulation of ²¹⁰Pb, *J. Geophys. Res.*, **98**, 20,573-20,586, 1993.
- Barth, M., P. J. Rasch, J. T. Kiehl, C. M. Benkovitz, and S. E. Schwartz, Sulfur chemistry in the National Center for Atmospheric Research Community Climate Model: Description, Evaluation, Features and Sensitivity to aqueous chemistry, *J. Geophys. Res.*, **105**, 1387-1415, 2000.
- Bates, T. S., B. K. Lamb, A. Guenther, J. Dignon, and R. E. Stoiber, Sulfur emissions from natural sources, *J. Atmos. Chem.*, **14**, 315-337, 1992.
- Benkovitz, C. M., M. T. Scholtz, J. Pacyna, L. Tarrason, J. Dignon, E. C. Voldner, P. A. Spiro, J. A. Logan, and T. E. Graedel, Global gridded inventories of anthropogenic emissions of sulfur and nitrogen, *J. Geophys. Res.*, **101**, 29,239-29,253, 1996.
- Berresheim, H., J. W. Huey, R. P. Thorn, F. L. Eisele, D. J. Tanner, and A. Jefferson, Measurements of dimethyl sulfide, dimethyl sulfoxide, dimethyl sulfone, and aerosols at Palmer Station, Antarctica, *J. Geophys. Res.*, **103**, 1629-1637, 1998.
- Bluth, G. J. S., W. I. Rose, I. E. Sprod, and A. J. Krueger, Stratospheric loading of sulfur from explosive volcanic eruptions, *J. Geology*, **105**, 671-683, 1997.
- Chin, M., D. J. Jacob, G. M. Gardner, M. S. Foreman-Fowler, and P. A. Spiro, A global three-dimensional model of tropospheric sulfate, *J. Geophys. Res.*, **101**, 18,667-18,690, 1996.
- Chin, M., and D. J. Jacob, Anthropogenic and natural contributions to tropospheric sulfate: A global model analysis, *J. Geophys. Res.*, **101**, 18,691-18,699, 1996.
- Chin, M., R. B. Rood, D. J. Allen, M. O. Andreae, A. M. Thompson, S.-J. Lin, R. M. Atlas, and J. V. Ardizzone, Processes controlling dimethyl sulfide over the ocean: Case studies using a 3-D model driven by assimilated meteorological fields, *J. Geophys. Res.*, **103**, 8341-8353, 1998.
- Chin, M., D. L. Savoie, B. J. Huebert, A. R. Bandy, D. C. Thornton, T. S. Bates, P. K. Quinn, E. S. Saltzman, and W. J. De Bruyn, Atmospheric sulfur cycle simulated in the global model GOCART: Comparison with field observations and regional budgets, submitted to *J. Geophys. Res.*, 2000.
- Chuang, C. C., J. E. Penner, K. E. Taylor, A. S. Grossman, and J. J. Walton, An assessment of the radiative effects of anthropogenic sulfate, *J. Geophys. Res.*, **102**, 3761-3778, 1997.
- Cohan, D. S., M. G. Schultz, D. J. Jacob, B. G. Heikes, D. R. Blake, Convective injection and photochemical decay of peroxides in the tropical upper troposphere: methyl iodide as a tracer of marine convection, *J. Geophys. Res.*, **104**, 5717-5724, 1999.
- Dana, M. T., and J. M. Hales, Statistical aspects of the washout of polydisperse aerosols, *Atmos. Environ.*, **10**, 45-50, 1976.
- Daum, P. H., S. E. Schwartz, and L. Newman, Acidic and related constituents in liquid-water clouds, *J. Geophys. Res.*, **89**, 1447-1458, 1984.
- DeMore, W. B., S. P. Sander, D. M. Golden, R. F. Hampson, M. J. Kurylo, C. J. Howard, A. R. Ravishankara, C. E. Kolb, and M. J. Molina, *Chemical Kinetics and Photochemical Data for Use in Stratospheric Modeling*, Evaluation Number 12, Jet Propulsion Laboratory, Cal. Tech., Pasadena, California, Jan. 1997.
- Erickson, D. J., III, A stability dependent theory for air-sea gas exchange, *J. Geophys. Res.*, **98**, 8471-8488, 1993.
- Feichter, J., E. Kjellstrom, H. Rodhe, F. Dentener, J. Lelieveld, and G.-J. Roelofs, Simulation of the tropospheric sulfur cycle in a global climate model, *Atmos. Environ.*, **30**, 1693-1708, 1996.
- Ganzeveld, L., J. Lelieveld, and G.-J. Roelofs, A dry deposition parameterization for sulfur oxides in a chemistry and general circulation model, *J. Geophys. Res.*, **103**, 5679-5694, 1998.
- Giorgi, F., and W. L. Chameides, Rainout lifetimes of highly soluble aerosols and gases as inferred from simulations with a general circulation model, *J. Geophys. Res.*, **91**, 14,367-14,376, 1986.
- Helfand, H. M., and J. C. Labraga, Design of a nonsingular level 2.5 second-order closure model for the pre-

- duction of atmospheric turbulence, *J. Atmos. Sci.*, **45**, 113-132, 1988.
- Huffman, G. J., et al., The Global Precipitation Climatology Project (GPCP) combined precipitation data set, *Bull. Amer. Meteorol. Soc.*, **78**, 5-20, 1997.
- Kettle, A. J., et al., A global database of sea surface dimethylsulfide (DMS) measurements and a simple model to predict sea surface DMS as a function of latitude, longitude and month, *Global Biogeochem. Cycles*, **13**, 399-444, 1999.
- Koch, D., D. Jacob, I. Tegen, D. Rind, and M. Chin, Tropospheric sulfur simulation and sulfate direct radiative forcing in the GISS GCM, *J. Geophys. Res.*, **104**, 23,799-23,823, 1999.
- Langner, J., and H. Rodhe, A global three-dimensional model of the tropospheric sulfur cycle, *J. Atmos. Chem.*, **13**, 225-263, 1991.
- Lin, S.-J., and R. B. Rood, Multidimensional flux-form semi-Lagrangian transport schemes, *Mon. Weather Rev.*, **124**, 2046-2070, 1996.
- Liss, P. S., and L. Merlivat, Air-sea gas exchange rates: Introduction and synthesis, in *The Role of Air-Sea Exchange in Geochemical Cycling*, pp. 113-127, edited by P. Buat-Ménard, D. Riedel, Norwell, Mass., 1986.
- McCormick, M. P., L. W. Thomason, and C. R. Trepte, Atmospheric effects of the Mt. Pinatubo eruption, *Nature*, **373**, 309-404, 1995.
- Müller, J.-F., and G. Brasseur, A three-dimensional chemical transport model of the global troposphere, *J. Geophys. Res.*, **100**, 16,445-16,490, 1995.
- Olivier, J. G. J., A. F. Bouwman, C. W. M. Van der Maas, J. J. M. Berdowski, C. Veldt, J. P. J. Bloss, A. J. H. Vesschedijk, P. Y. J. Zandveld, and J. L. Haverlag, Description of EDGAR Version 2.0. A set of global emission inventories of greenhouse gases and ozone-depleting substances for all anthropogenic and most natural sources on a per country basis and on $1^\circ \times 1^\circ$ grid, *RIVM/TNO report 771060 002*, RIVM, Bilthoven, Dec. 1996.
- Pham, M., J.-F. Müller, G. Brasseur, C. Granier, and G. Megie, A three-dimensional study of the tropospheric sulfur cycle, *J. Geophys. Res.*, **100**, 26,061-26,092, 1995.
- Rasch, P. J., M. C. Barth, J. T. Kiehl, S. E. Schwartz, and C. M. Benkovitz, A description of the global sulfur cycle and its controlling processes in the National Center for Atmospheric Research Community Climate Model, Version 3, *J. Geophys. Res.*, **105**, 1367-1385, 2000.
- Roelofs, G.-J., J. Lelieveld, and L. Ganzeveld, Simulation of global sulfate distribution and the influence on effective cloud drop radii with a coupled photochemistry-sulfur cycle model, *Tellus*, **50B**, 224-242, 1998.
- Saltzman, E. S., D. B. King, K. Holmen, and C. Leck, Experimental determination of the diffusion coefficient of dimethylsulfide in seawater, *J. Geophys. Res.*, **98**, 16,481-16,486, 1993.
- Sandnes, H., and H. Styve, Calculated budgets for airborne acidifying components in Europe, 1985, 1987, 1988, 1989, 1990 and 1991. *EMEP/MS-CW Report 1/92*. The Norwegian Meteorological Institute, Oslo, Norway, 1992.
- Schnetzler, C. C., G. J. S. Bluth, A. J. Krueger, and L. S. Walter, A proposed volcanic sulfur dioxide index (VSI), *J. Geophys. Res.*, **102**, 20,087-20,091, 1997.
- Schubert, S. D., R. B. Rood, and J. Pfendtner, An assimilated data set for earth science applications, *Bull. Amer. Meteorol. Soc.*, **74**, 2331-2342, 1993.
- Smethie, W. M. Jr., T. Takahashi, D. W. Chipman, and J. R. Ledwell, Gas exchange and CO_2 flux in the tropical Atlantic Ocean determined from ^{222}Rn and pCO_2 measurements, *J. Geophys. Res.*, **90**, 7005-7022, 1985.
- Smikin, T., and L. Siebert, *Volcanoes of the World*, 2nd ed., Geoscience Press, Tucson, Arizona, 1994.
- Staubs, R., and H.-W. Georgii, Biogenic sulfur compounds in seawater and the atmosphere of the Antarctic region, *Tellus*, **45B**, 127-137, 1993.
- Sundqvist, H., E. Berge, and J. E. Kristiansson, Condensation and cloud parameterization studies with a mesoscale numerical weather prediction model, *Mon. Weather Rev.*, **117**, 1641-1657, 1989.
- Suzuki, T., A theoretical model for dispersion of tephra, in *Arc Volcanism: Physics and Tectonics*, edited by D. Shimozuru and I. Yokoyama, pp. 95-113, 1983.
- Takacs, L. L., A. Molod, and T. Wang, Documentation of the Goddard Earth Observing System (GEOS) general circulation model - version 1, *NASA Tech. Memo.*, *TM-104606*, vol. 1, 1994.
- Tarrason, L., and T. Iversen, Modeling intercontinental transport of atmospheric sulphur in the northern hemisphere, *Tellus*, **50B**, 331-352, 1998.
- Voldner, E. C., L. A. Barrie, and A. Sirois, A literature review of dry deposition of oxides of sulphur and nitrogen with emphasis on long-range transport modelling in North America, *Atmos. Environ.*, **20**, 2101-2123, 1986.
- Walcek, C. J., R. A. Brost, J. S. Chang, and M. L. Wesely, SO_2 , sulfate and HNO_3 deposition velocities computed using regional landuse and meteorological data, *Atmos. Environ.*, **20**, 949-964, 1986.
- Wanninkhof, R., Relationship between wind speed and gas exchange over the ocean, *J. Geophys. Res.*, **97**, 10,757-10,768, 1992.
- Weisenstein, D. K., M. K. W. Ko, N.-D. Sze, and J. M. Rodriguez, Potential impact of SO_2 emissions from stratospheric aircraft on ozone, *Geophys. Res. Lett.*, **23**, 161-164, 1996.
- Wesely, M. L., and B. B. Hicks, Some factors that affect the deposition rates of sulfur dioxide and similar gases on vegetation, *J. Air Pollut. Contr. Assoc.*, **27**, 1110-1116, 1977.
- Wesely, M. L., Parameterization of surface resistance to gaseous dry deposition in regional-scale numerical mod-

els. *Atmos. Environ.*, *23*, 1293-1304, 1989.

Xu, K.-M., and S. K. Krueger, Evaluation of cloudiness parameterizations using a cumulus ensemble model, *Mon. Weather Rev.*, *119*, 342-367, 1991.

M. Chin, NASA Goddard Space Flight Center, Code 916, Greenbelt, Maryland, 20771. (email: chin@rondo.gsfc.nasa.gov)

S.-J. Lin, R. B. Rood, and A. M. Thompson, NASA Goddard Space Flight Center, Greenbelt, Maryland, 20771. (email: rood@dao.gsfc.nasa.gov; slin@dao.gsfc.nasa.gov; thompson@gator1.gsfc.nasa.gov)

J.-F. Müller, Belgian Institute for Space Aeronomy, Brussels, Belgium. (email: Jean-Francois.Muller@bira-iasb.oma.be)

Received —; revised —; accepted —.

¹School of Earth and Atmospheric Sciences, Georgia Tech, Atlanta, Georgia

²NASA Goddard Space Flight Center, Greenbelt, Maryland

³Belgian Institute for Space Aeronomy, Brussels, Belgium

Figure 1. Annual emissions ($\text{mg S m}^{-2} \text{ yr}^{-1}$) of 1990 for sulfate precursors from anthropogenic and natural (oceanic and volcanic) sources used in the model.

Figure 2. Zonal averaged distributions of OH and H_2O_2 for January and July from the IMAGES model [Müller and Brasseur, 1995].

Figure 3. Summary of a 6-year sulfur budget (1989-1994) in the GOCART model. Troposphere and stratosphere interface at 120-100 mb.

Figure 4. Distributions of sulfur species (ppt) in for DJF and JJA in 1990 at (a) the surface and (b) 500 mb.

Figure 5. Zonal distributions of sulfur species (ppt) in the simulation for 1990.

Figure 6. Sources and sinks for sulfate in the 1990 simulation as a function of latitude.

Figure 7. Total sulfate column burden (mg S m^{-2}) and the anthropogenic fraction in the 1990 simulation.

Figure 8. Zonally averaged anthropogenic sulfate fraction in DJF and JJA for 1990.

Table 1. GEOS-DAS meteorological fields used in GOCART

GEOS-DAS fields

Prognostic fields (instantaneous value, every 6 hours):

- Surface pressure
- Temperature
- Wind velocity
- Specific humidity
- Surface albedo
- Surface type (land, water, or ice)

Diagnostic fields (average value, every 3 or 6 hours):

- Cloud mass flux
- Convective cloud detrainment
- Cloud fraction (column)
- Specific humidity change
- Total precipitation at the surface
- Convective precipitation at the surface
- Aerodynamic resistance
- Surface friction velocity
- Surface roughness length
- Surface air temperature
- Surface sensible heat flux
- Boundary layer depth
- Wind velocity at 10 m
- Turbulent diffusion coefficient^a
- Net shortwave radiation at the surface

^aTurbulent diffusion coefficients were not archived in the earlier version of GEOS-DAS (before 1997). They have been calculated using the archived GEOS DAS fields for simulations before 1997.

Table 2. Comparison of Sulfur Budget from the GOCART Model with The GISS and NCAR Models.

Budget Component	GOCART ^a		GISS ^b		NCAR ^c	
Total emission (Tg S yr ⁻¹)	93.9		83.0		82.5	
SO ₂ anthropogenic	70.6	(75.2%)	64.6	(77.8%)	65.7	(79.6%)
SO ₂ biomass burning	2.3	(2.4%)	2.3	(2.8%)		
SO ₂ volcanic	5.5	(5.9%)	3.5	(4.2%)		
Sulfate anthropogenic	2.2	(2.3%)	1.9	(2.3%)		
DMS oceanic	13.3	(14.2%)	10.7	(12.9%)	15.5	(18.8%)
Total deposition (Tg S yr ⁻¹)	93.0		83.4		81.0	
SO ₂ dry deposition	41.2	(44.3%)	35.5	(42.6%)	24.5	(30.2%)
SO ₂ wet scavenging	10.6	(11.4%)	0.2	(0.2%)	1.6	(2.0%)
Sulfate dry deposition	5.1	(5.5%)	9.2	(11.0%)	3.7	(4.6%)
Sulfate wet scavenging ^d	34.7	(37.3%)	37.4	(44.8%)	51.2	(63.2%)
MSA dry deposition	0.1	(0.1%)	0.2	(0.2%)		
MSA wet scavenging	1.3	(1.4%)	0.9	(1.1%)		
SO ₂ production (Tg S yr ⁻¹)	11.9		10.0		15.5	
From DMS+OH	10.4	(87.4%)				
From DMS+NO ₃	1.5	(12.6%)				
Sulfate production (Tg S yr ⁻¹)	38.5		44.7		53.6	
In-air	14.0	(36.4%)	3.1	(29.3%)	9.2	(17.2%)
In-cloud ^d	24.5	(63.6%)	31.6	(70.7%)	4.4	(8.2%)
Burden (Tg S)						
SO ₂	0.43		0.56		0.4	
Sulfate	0.63		0.73		0.57	
DMS	0.073		0.056		0.06	
MSA	0.028		0.023			
Lifetime (days)						
SO ₂	1.8		2.6		1.9	
Sulfate ^e	5.8	(4.6)	5.7		4.0	
DMS	2.0		1.9		1.4	
MSA	7.1		7.6			
Loss frequency ^f (day ⁻¹)						
SO ₂ dry deposition	0.26		0.17		0.17	
SO ₂ in-air oxidation	0.09		0.06		0.06	
SO ₂ in-cloud oxid.+wet scav.	0.22		0.15		0.31	
Sulfate dry deposition	0.02		0.03		0.02	
Sulfate wet scavenging	0.15	(0.2)	0.14		0.25	

^aThis work, 1990 simulation.

^bKoch *et al.*, [1999].

^c*Barth et al., [2000]; Rasch et al., [2000]*.

^dSO₂ wet scavenging is counted as a part of sulfate in-cloud production and sulfate wet scavenging in the GISS and NCAR model. See text for details.

^eThe numbers in parentheses for the GOCART model are the values that would be if SO₂ wet scavenging were considered as a part of sulfate wet deposition term, as treated by the GISS and NCAR models. See text for explanation.

^fLoss frequency is defined as the loss rate divided by the burden.

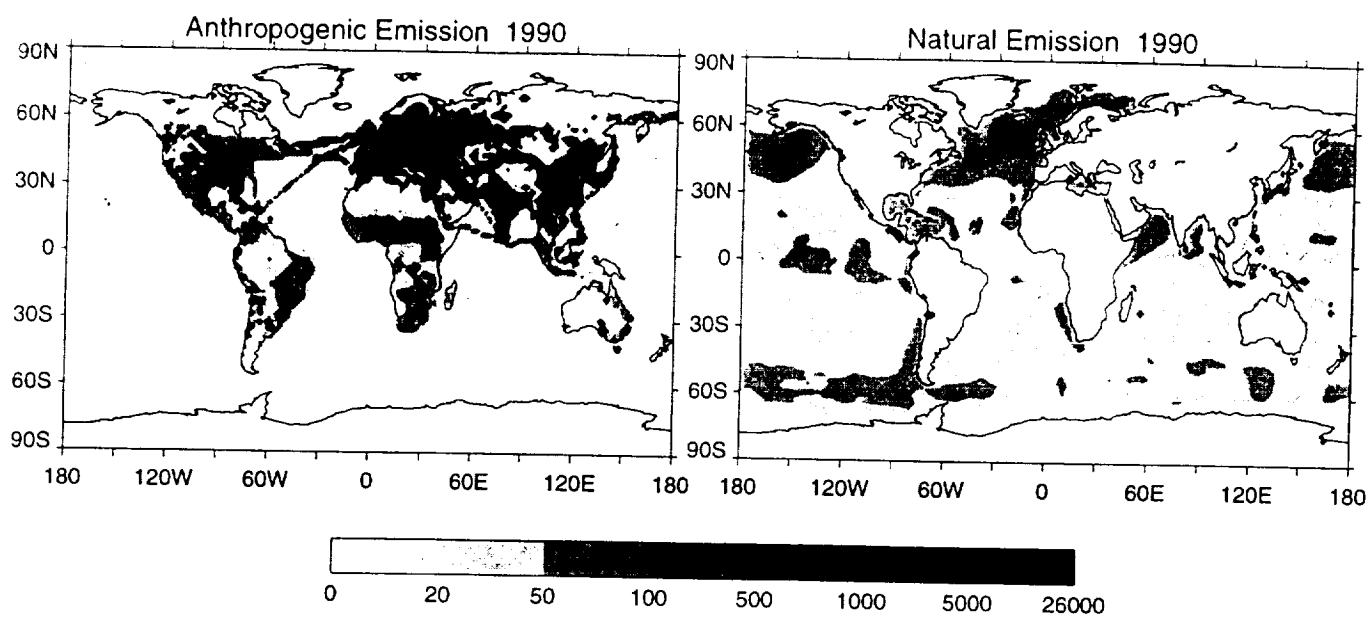


Figure 1

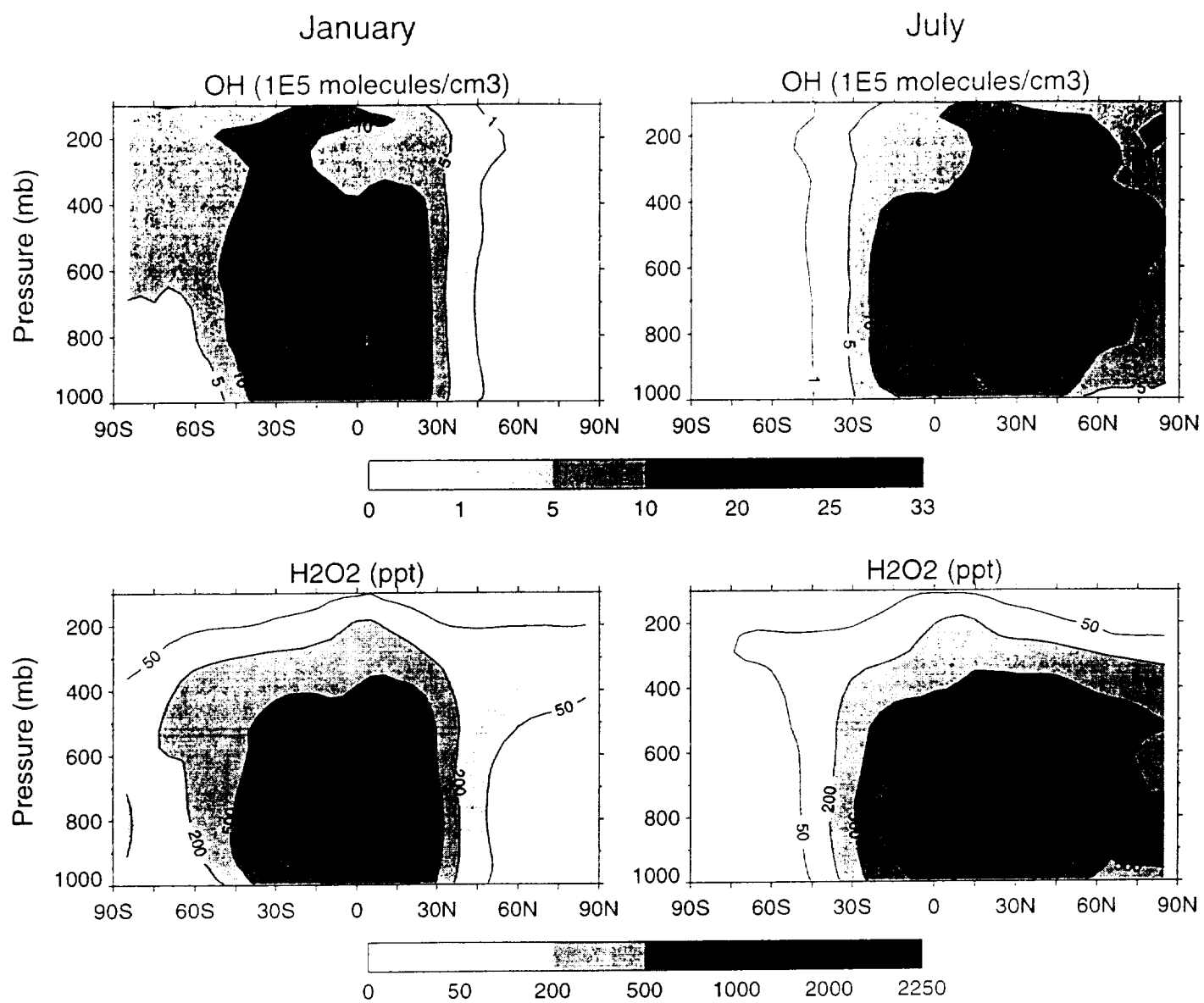


Figure 2

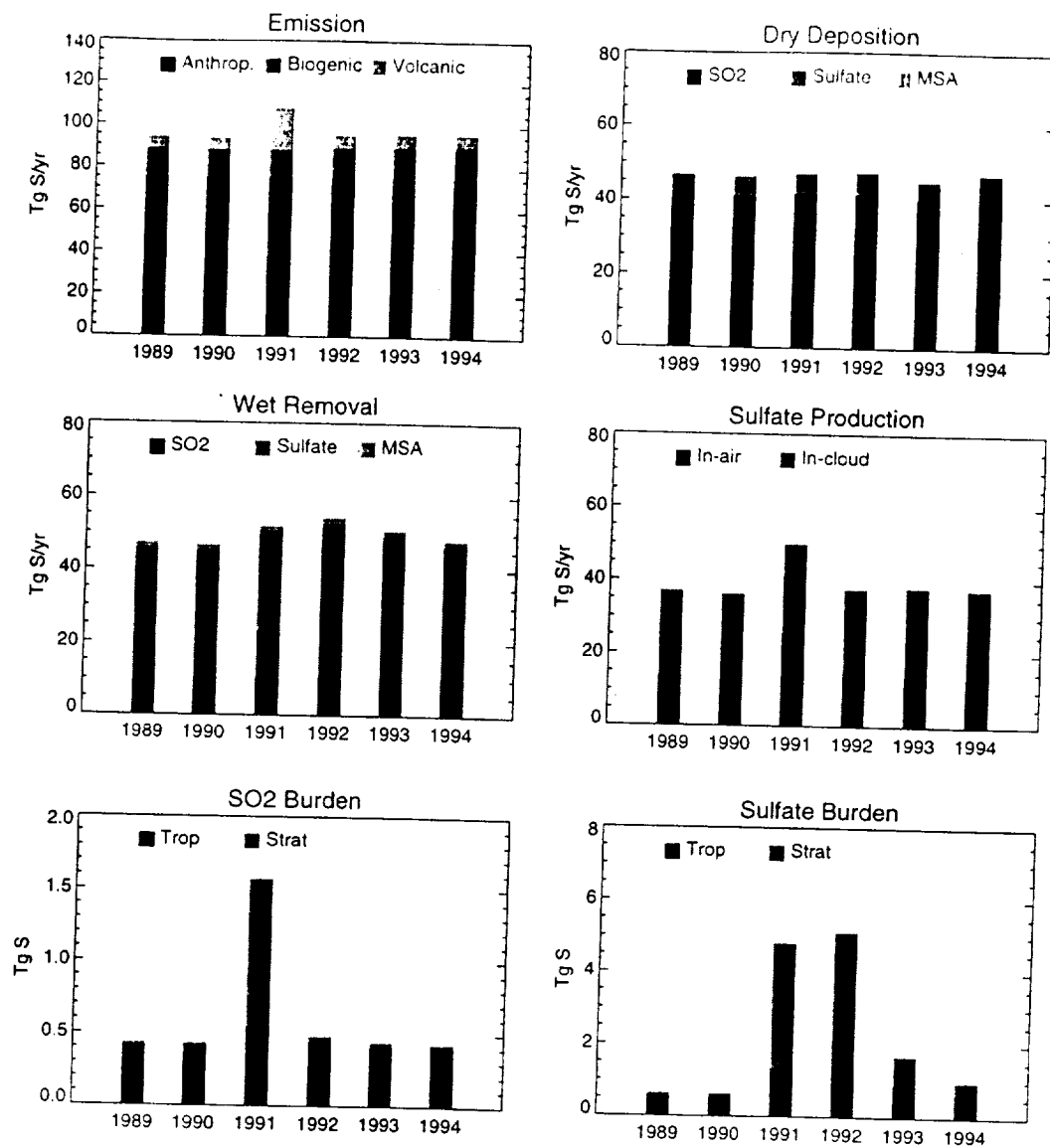


Figure 3

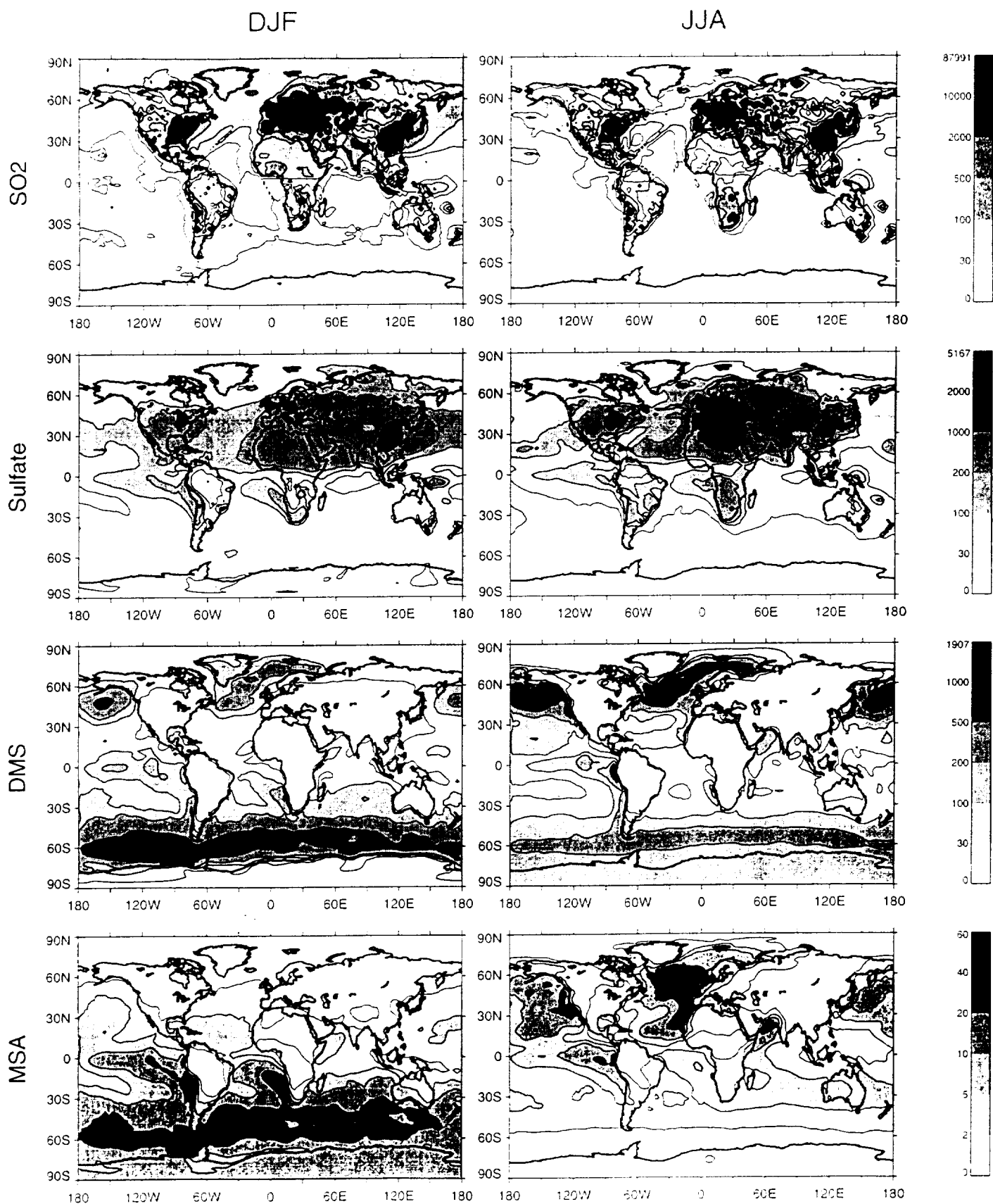


Figure 4a

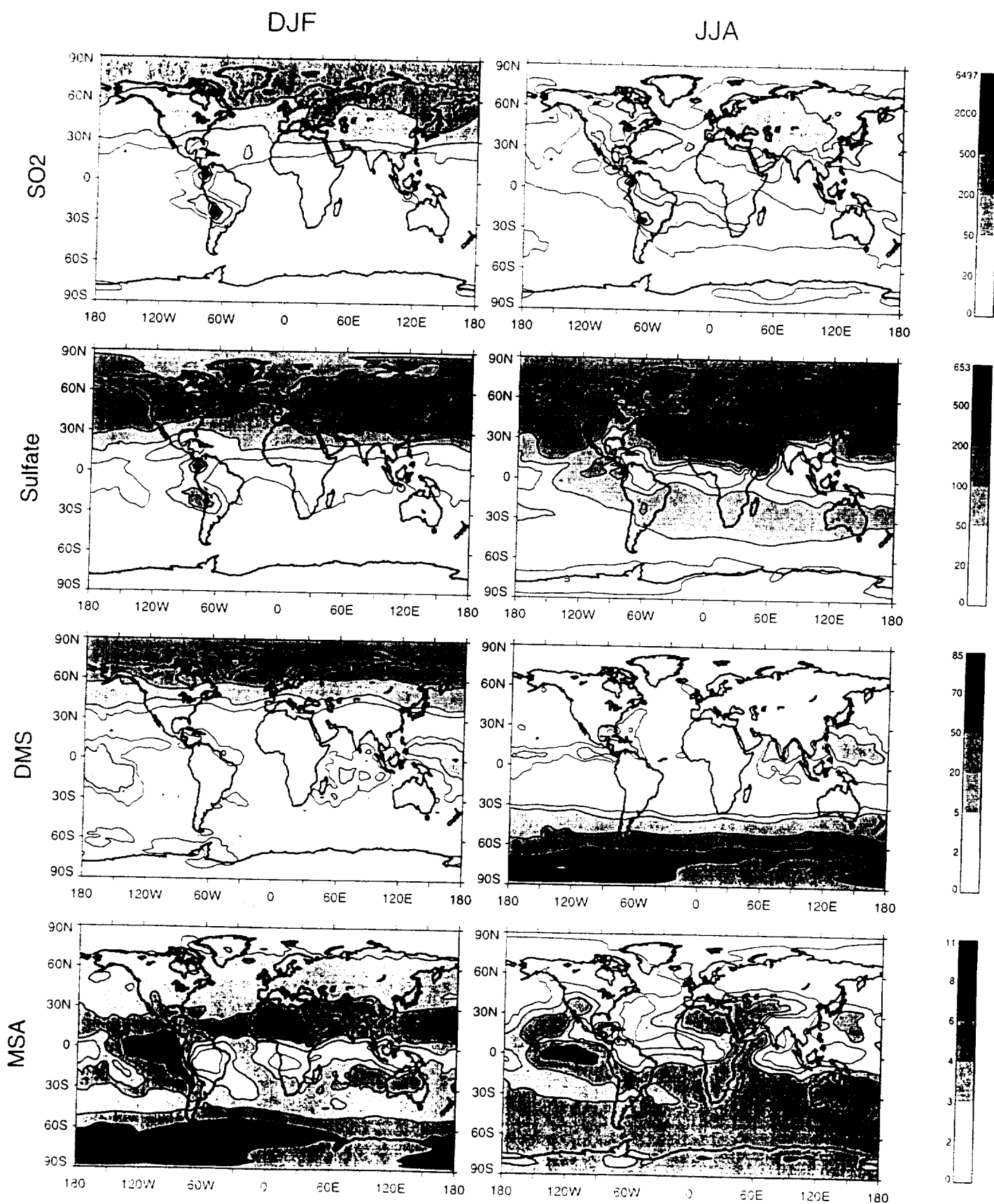


Figure 4b

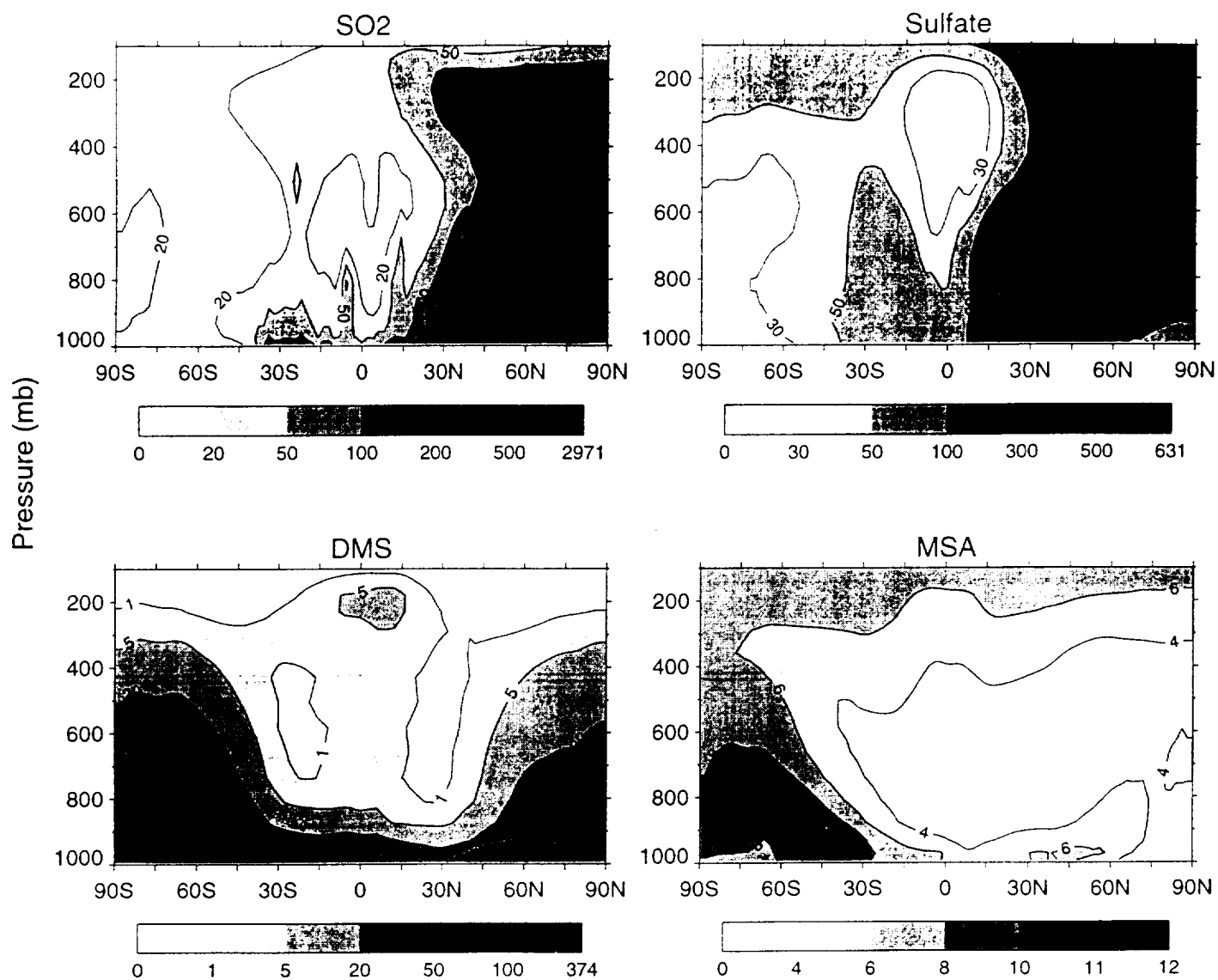


Figure 5

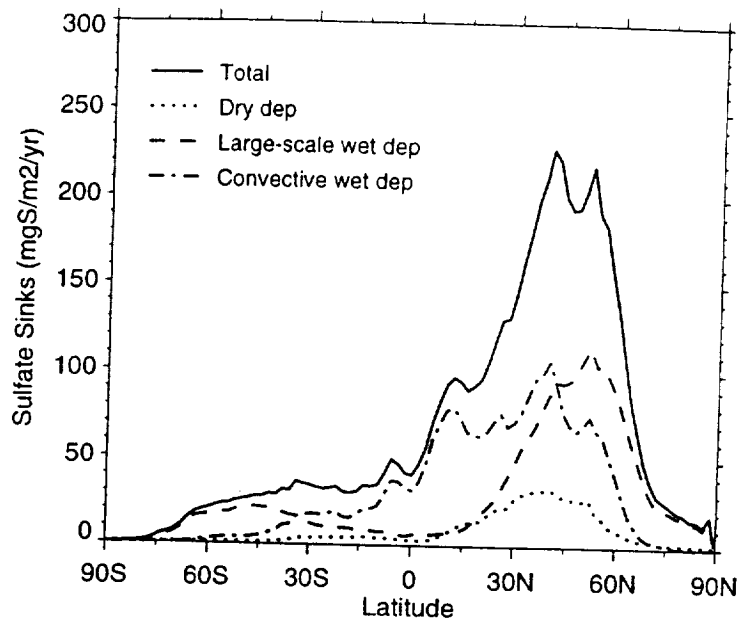
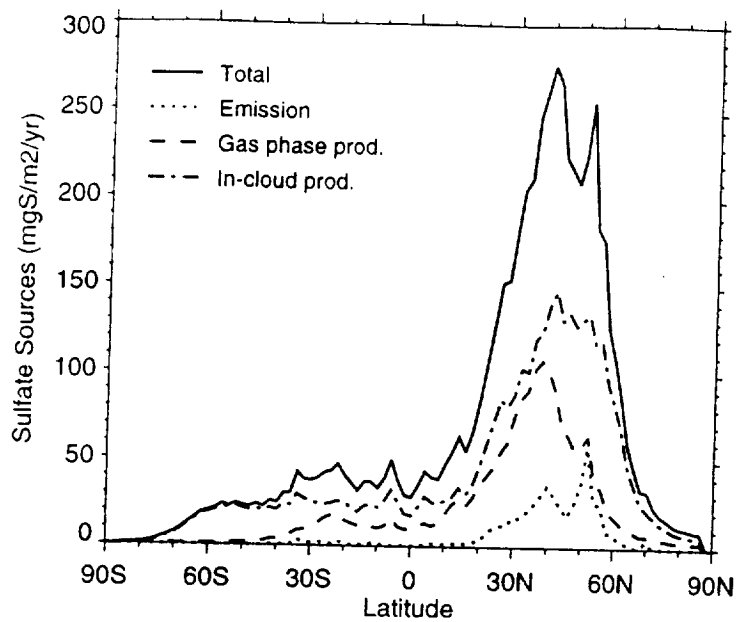


Figure 6

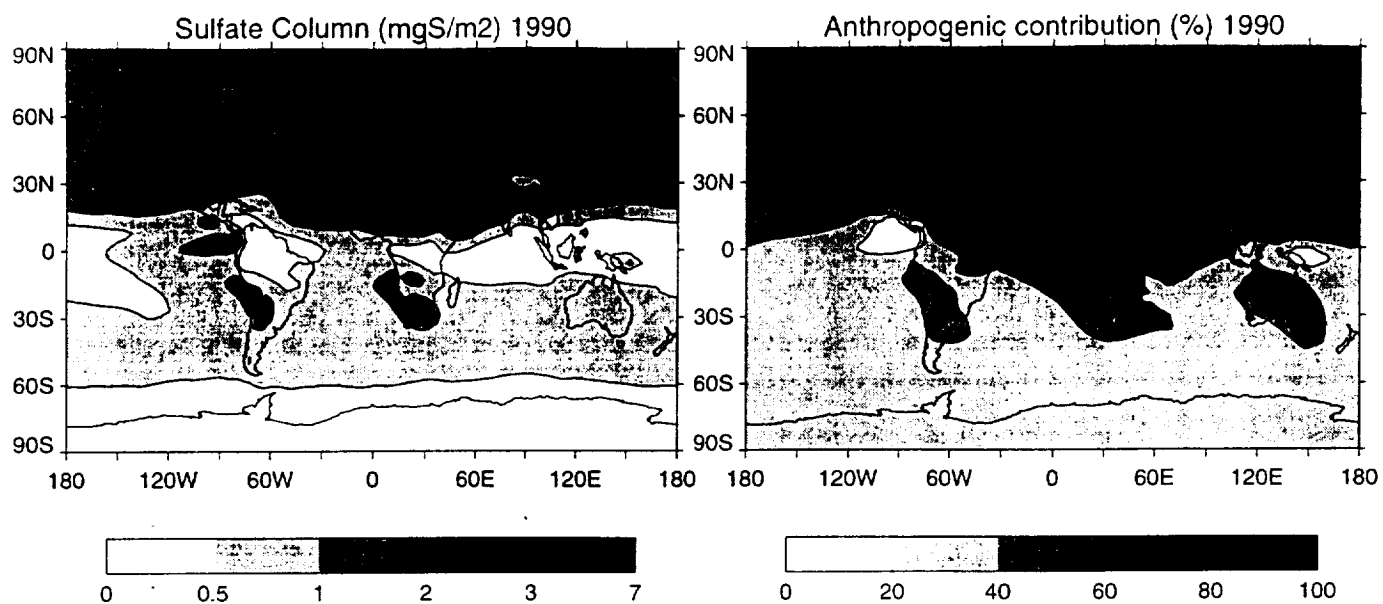


Figure 7

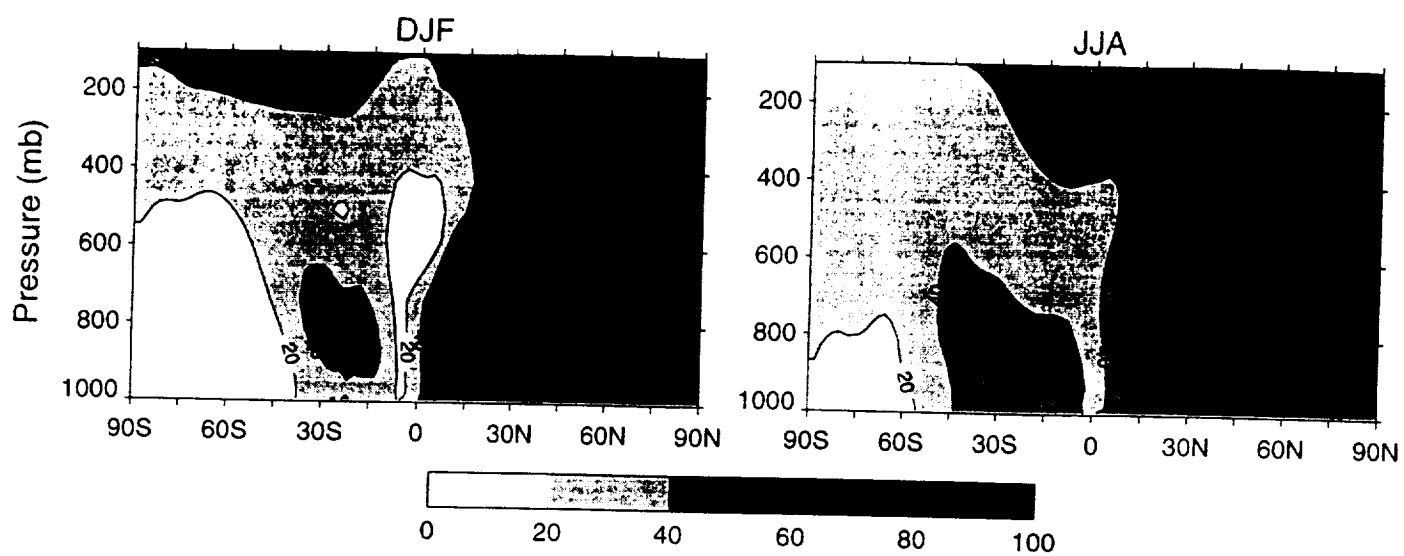


Figure 8